Spring 2019

Solid State Polyaniline Supercapacitors Based on Electrodes Fabricated with Electropolymerization

Jonathan R. Blincoe
Old Dominion University

SOLID STATE POLYANILINE SUPERCAPACITORS BASED ON ELECTRODES FABRICATED WITH ELECTROPOLYMERIZATION

by

Jonathan R. Blincoe
B.S. May 2016, Old Dominion University

A Thesis Submitted to the Faculty of
Old Dominion University in Partial Fulfillment of the
Requirements for the Degree of

MASTER OF SCIENCE

ELECTRICAL AND COMPUTER ENGINEERING

OLD DOMINION UNIVERSITY
April 2019

Approved by:

Gon Namkoong (Director)

Hani Elsayed-Ali (Member)

Helmut Baumgart (Member)

ABSTRACT

SOLID STATE POLYANILINE SUPERCAPACITORS BASED ON ELECTRODES FABRICATED WITH ELECTROPOLYMERIZATION

Jonathan R. Blincoe
Old Dominion University, 2019
Director: Dr. Gon Namkoong

Supercapacitors are energy storage devices with the potential to overshadow lithium-ion batteries in the energy storage sector. Generally supercapacitors store less energy than a lithium-ion battery, but make up for it with much higher power densities that allow supercapacitors to charge and discharge quickly. This can be through the formation of an electric double layer or faradaic phenomenon between the electrode and electrolyte. The energy storage mechanism relies heavily on the electrode material and the ions contained within the electrolyte. In this research, polyaniline was used as an active material to prepare supercapacitors. Polyaniline is a conductive polymer that is redox active and can be fabricated to be highly porous, making it an excellent choice for supercapacitors. It was found that a specific concentration of precursor solution containing aniline in diluted sulfuric acid could be electropolymerized at an optimized voltage of 1.21V to form an anodic deposit of polyaniline capable of 612 F/g in a half-cell with standard 1M H_2SO_4 electrolyte. This can be enhanced with hydroquinone as a redox mediator, causing the half-cell to exhibit 3,416 F/g on average with 0.1M hydroquinone added to the electrolyte. This design was further tested in a full cell with aqueous electrolyte and polyvinyl alcohol electrolyte. The final design iteration is a symmetric solid state supercapacitor with polyvinyl alcohol electrolyte containing hydroquinone. The completed device exhibited 307 F/g on average.

ACKNOWLEDGMENTS

I would like to first thank people who have had an impact on my life as well as those who have helped with my research afterwards. First of all, my parents and my family have always been there for me and have helped me grow into the man I am today. I am grateful for everything they have done for me. Second, I appreciate my friends who have been with me through the thick and thin and have listened to me drone on about material physics. Of these friends I am especially thankful for Dominic, Andrew, and Collin. Finally, my beautiful girlfriend Amber has been there through my entire graduate career and has never given up on me even when I feel like giving up myself.

Now I would like to thank all those that helped me with my research. Thank you to my advisor Dr. Namkoong for giving me this opportunity and letting me work in the lab. Mamun, I really appreciate all the guidance in the lab and all the help you gave me. I could not have done it without you or Tanzilla, who did an excellent job characterizing samples with the machines only doctorate students have access to and taught me to use most of the others. I also appreciate everyone else who allowed me to use their equipment and/or taught me to use equipment including Dr. Baumgart, Dr. Cao, Dr. Ali, Dr. Kelley, Dr. Fattah, Nizam, and Kory. Thank you to Yun who helped manage the lab and helped me out with whatever she could.

I would also like to thank my peers Wayne and Daniel for discussing theoretical implications of design and performance. Discussing these topics with others helped shed light on missed details. Wayne was always willing to field any questions I may have regarding supercapacitors, shared his lab experience to help me with information I cannot simply read about in literature, and generally challenged my understanding to push it further. Both of you were instrumental to my development as a researcher. Shout out to Alexandra Elbakyan, a true hero who champions knowledge for all. The

world is a better place with people like you.

Finally I want to thank all the people who have inspired me or went above and beyond to help me (in no particular order): Dr. Behson, Dr. Bailey, Dr. Vahala, Deb, Elon Musk, Matt ODowd, Brian Greene, Tad Hussey, Rick Sanchez, and all other scientists who have inspired me or helped me understand nature.

TABLE OF CONTENTS

LIST OF FIGURES

CHAPTER 1

INTRODUCTION

Research and growth in clean, renewable energy generation demands a great need for inexpensive, green energy storage to limit the human impact on climate change. Lithium-ion batteries currently dominate the energy storage market but can be dangerous and charge slowly. Supercapacitors are devices that can quickly store a massive amount of energy and deliver high power. While batteries typically store more energy, research is leading towards the next generation of energy storage devices- supercapacitors with energy densities comparable to lithium-ion batteries. Solar power in particular needs supercapacitors capable of safely storing the excess energy produced during the day to power homes and charge electric vehicles. Electric vehicles can benefit from supercapacitors as they require both bursts of high power output and a massive energy storage to maximize the travel distance on a full charge and for things such as acceleration and regenerative braking. Current electric vehicles feature lithium-ion batteries which are heavy, charge slowly, and can be extremely dangerous. A typical supercapacitor exhibits an order of magnitude lower energy density and two orders of magnitude higher power density than lithium-ion batteries. This means the supercapacitor is capable of charging three orders of magnitude faster. Additionally, lithium-ion batteries have fairly low cycle stability while new supercapacitive devices feature retention of over 95 percent and exhibit stable behavior for two to three orders of magnitude more cycles than of batteries [1]. Supercapacitors are also desirable for wearable electronics as they can be lightweight and flexible.

Supercapacitors differ from normal capacitors as they employ porous materials with high surface areas to store charge throughout a volume of active electrode

material. The maximum theoretical capacitance assumes that every bit of active material is able to participate in the reaction. Realistically, this is not the case as only the outer layers of material are active. This urges the importance of the materials morphology to have the optimal surface area exposure while still maintaining a stable structure. As a result, electrodes with thin films of active material generally operate the best. A thicker film might accumulate a high electrical or ionic resistance, leading to poor performance, while requiring more material cost.

It is important to note that while expensive production methods can be used to build extremely high functioning devices, there is a greater need for low-cost mass production of reasonably high functioning devices to satisfy the power needs of electronics using lithium-ion batteries for energy storage. The goal of this thesis was to formulate a scalable electrochemical fabrication technique for low-cost mass production of supercapacitor electrodes.

1.1 ELECTROCHEMICAL SUPERCAPACITORS

Electrochemical supercapacitors store energy through Faradaic charge transfer between the electrode and the electrolyte. The reaction can be either capacitive or non-capacitive, where the Faradaic devices that exhibit capacitive charge storage are deemed pseudocapacitive [2]. Pseudocapacitive materials exhibit electrochemical signatures similar to EDL capacitors, while non-capacitive mechanisms result in sharp peaks that arise at specific potentials [3], [4]. The non-capacitive process are generally expressed by the Nernst equation and can be referred to as Nernstian processes [2]. Either way, the charge storage mechanism must cycle reversibly to be effective. The different ways are through redox reactions, intercalation, or electrosorption [5]. A basic representation of a redox reaction is expressed as:

$$O + ne^- \Longleftrightarrow R \tag{1}$$

where the oxidized species O requires n electrons to oxidize from the reduced form R [6]. The Gibbs free energy change ΔG, measured in J mol^{-1}, in an electrochemical cell is related to the standard free energy change ΔG^0 and the change in concentrations of O and R by:

$$\Delta G = \Delta G^0 + RTln\left(\frac{[R]}{[O]}\right) \tag{2}$$

In the equation, R is the gas constant (8.3145 J mol^{-1} K^{-1}) and T is the temperature (K). The free energy change ΔG is an important thermodynamic parameter that provides insight into the exchange of energy within a system depending on a systems enthalpy and entropy at a given temperature [7]. A spontaneous reaction occurs when the value is negative. A positive value means work is gained by the system, which can be related to redox mechanisms by the total number of electrons passed n and the electromotive force E of the cell [8]:

$$\Delta G = -nEF \tag{3}$$

where Faradays constant F is the charge passed by one mole of electrons (1F = 96485 C mol^{-1}). The electromotive force in this case is the potential between the electrodes [6].The standard free energy change ΔG^0 is related to the standard electrode potential E^0 as well:

$$\Delta G^0 = -nE^0F \tag{4}$$

The previous three equations together can then be used to derive the well-known Nernst equation, which relates the potential of the electrochemical cell with the degree of oxidation:

$$E = E^0 + \frac{RT}{nF} ln \left(\frac{[O]}{[R]} \right) \qquad (5)$$

An early relationship between the charge transferred and the amount of material was established when Faraday published what would one day be known as Faradays laws of electrolysis in 1834 [9]. The laws describe that the amount of charge transferred can be found based on the directly proportional to the number of electrons transferred [10]:

$$Q = mnF \qquad (6)$$

where Q is the electrochemical charge associated with a number of active species in moles (m) each gaining or losing a certain number of electrons (n).

The most commonly used metric for comparing supercapacitors is the specific capacitance [11]. The specific capacitance is the capacitance per measured unit, whether gravimetric (F g^{-1}), volumetric (F mL^{-1}), areal (F cm^{-2}), linear (F cm^{-1}), or normalized (F cm^{-1}). Equation 6 can be modified to represent the capacitance that arises from this reaction. The capacitance is then calculated based on the ratio between the amount of charge accumulated and the potential window of the reaction [12]:

$$C = \frac{mnF}{\Delta E} = \frac{Q}{\Delta E} \qquad (7)$$

The energy density is the amount of total energy the device can store at once. The energy density $E(J)$ can be determined based on the capacitance C and the operating voltage range V [13]:

$$E(J) = \frac{CV^2}{2} = \frac{QV}{2} \qquad (8)$$

In this equation, the capacitance can either be the specific capacitance or the total capacitance to result in the specific energy density and the total energy density respectively. Additionally, the specific energy density can be found by dividing the total energy density by the active weight of the device. This is the same in regards to the power density, which is a measure of the power that can be exerted by the device.

The power density P is based on the maximum voltage V across the device when fully charged and the equivalent series resistance R_S of the device [13]:

$$P = \frac{V^2}{4R_s} \tag{9}$$

The specific energy density is typically measured in watt hours per kilogram (Wh kg^{-1}) and the specific power density in watts per kilogram (W kg^{-1}). The energy equation above must be divided by 3600 to convert joules to Wh. Notice also the only difference between the units for energy density and the power density is time. The charge time can then be estimated roughly as the energy density divided by the power density. Energy storage devices can then be compared on the basis of a Ragone plot which plots the energy density against the power density with diagonal lines marking charge times.

Typically, batteries have higher energy densities while supercapacitors have higher power densities. For now, this means batteries and supercapacitors are potentially useful for different applications, but research in supercapacitor technology is closing the gap with high energy density supercapacitors. A few examples being an asymmetric supercapacitor in an aqueous electrolyte with an energy density of 66.4 Wh kg^{-1} [14], an asymmetric supercapacitor in an organic electrolyte 80.4 Wh kg^{-1} [15], and a lithium-based asymmetric supercapacitor using a common battery electrolyte

achieved an energy density of 157.5 Wh kg^{-1} [16]. That is higher than many commercial batteries, but is only just beginning to compete with current lithium-ion battery research which has attained over 800 Wh kg^{-1} [17]. The power densities are not quite as comparable between the two. Supercapacitors operate with power densities on the scale of 10^4 W kg^{-1} and even higher for those focusing on optimizing specific power. An example is a ruthenium, graphene, and carbon nanotube hybrid foam based symmetric supercapacitor with an aqueous electrolyte that achieved 128 kW kg^{-1} [18]. Batteries are often less than 1 kW kg$_{-1}$, but can be designed to reach 10 kW kg^{-1} for high power needs [17].

The resistances existing within a supercapacitor will all result in energy losses in some form. The two significant resistances being the electrical resistance and the forces acting upon an ion traveling through porous media [19]. Regardless of the energy storage mechanism, electrons lose energy across material interfaces and when traveling through conductive materials. Losses also result from electrolyte ions moving through or interacting with a porous substrate. A higher electrolyte viscosity or an extremely dense pore structure can result in higher resistances [20]. In depth discussions about modeling the behavior of electrochemical supercapacitors can be found in a paper by P. Guillemet, et al. or Conways book [3], [21].

1.1.1 POLYANILINE SUPERCAPACITORS

Polyaniline (PANI) is a conductive polymer that is heavily researched for energy storage due to its unique properties, low manufacturing cost, environmental stability [22], and design flexibility [23]. PANI is also a useful material for sensors [24], solar cells [25], and electrochromic devices [26]. To fully understand how and why PANI is useful for these applications, one should first understand the structure of the polymer chains and how they form.

Polyaniline can be represented in general by Figure 1, where the polymer chain
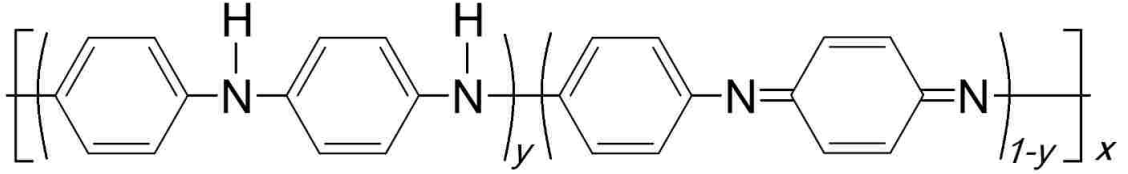
FIG. 1: The basic repeating unit of polyaniline.

contains y reduced groups and $(1-y)$ oxidized groups repeated x times [27]. Polyaniline is often referenced as one of three forms based on the degree of oxidation. The form containing only reduced groups ($y = 1$) with amine groups connecting benzenoid rings is called leucoemeraldine, the fully oxidized form ($y = 0$) with imine groups connecting alternating benzenoid and quinonoid rings is referred to as pernigraniline, and the emeraldine form ($y = 0.5$) is the middle stage with equal reduced and oxidized groups. This change in oxidation state causes a change in band energy, which causes this material to be electrochromic.

Part of the massive interest in polyaniline stems from the ability to protonate the nitrogen sites along the backbone of the polymer chain with acids to increase conductivity [28], [29]. This is because the protonation of H+ adds holes that cause delocalization, and the degree of delocalization has a direct effect on the conductivity since conductivity is related to charge carrier mobility [29], [30]. Protonation will occur when the pH of an aqueous acid solution is less than 4 and will form mostly salt form when pH is near 0 [28]. Protonation is favored at imine sites until about half of the sites are protonated, then internal redox mechanisms cause the double-bonds to reorganize [29], [31]. The fully protonated emeraldine salt takes the form shown in Figure 2 in which X- is the ion from the acid HX [27], [31], [32].

Polyaniline can also be doped with various ions in solution to result in varying levels of conductivity [28], [33]. Emeraldine experiences the most change in conductivity from ion doping when compared to pernigraniline and leucoemeraldine, and
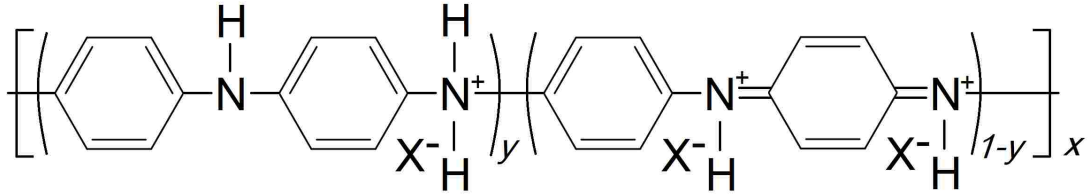
FIG. 2: The repeating unit of the protonated form, emeraldine salt.

protonated emeraldine is capable of achieving the highest conductivity [33][34][35]. Because of this, most research on polyaniline as a supercapacitor, or anything conductive for that matter, has been focused on emeraldine salts [22][36][37]. Polyaniline half-oxidized to the emeraldine state is also extremely useful for sensors due to the wide conductivity range as a result of changes in delocalization behavior.

The emeraldine salt form has been made in many ways other than aqueous acid doping emeraldine base. A pernigraniline film treated with a dilute aqueous acid will protonate and reduce to the emeraldine form in the process [33]. Additionally placing a pernigraniline film and a leucoemeraldine film together can cause the pernigraniline film to be reduced by the leucoemeraldine film as the leucoemeraldine film is oxidized by the pernigraniline film [38]. To mediate this process more effectively, water and other polar solvents have been shown to help redistribute charge along the backbone of the polymer to increase conductivity throughout the sample [30]. These mechanics are important for reducing waste and recycling material to lower manufacturing costs and environmental impact.

Earlier in this section, polyaniline was mentioned to be electrochromic. This means that the application of electric potential changes the optical properties of polyaniline due to a change in oxidation state [39]. Many researchers have thoroughly documented the spectral peaks produced by polyaniline at its various states, including emeraldine doped with various acids and ions [29][33][40][41]. Since peaks in the visible range are shifted, it is common to describe the state with the color

seen by the naked eye [42]. The colors of the films to the naked eye are as follows: fully reduced leucoemeraldine base is colorless/transparent yellow, emeraldine base is blue, pernigraniline base is violet, emeraldine salt is green, and pernigraniline salt is dark blue/black [35], [39], [42].

1.2 ELECTROPOLYMERIZATION OF POLYANILINE

In this experiment the polymer is formed through electropolymerization, but many researchers investigate polyaniline using hydrothermal synthesis [43] or chemical oxidation [44]. In any case, there are a multitude of parameters (temperature, voltage, duration, oxidant, etc.) that affect the morphology of the film, but this thesis will focus on polyaniline fabricated through electropolymerization. Electropolymerization is attractive to researchers due to its fine control of processing along with cleaner results requiring less chemicals [45]. The electropolymerization process typically begins with the aniline monomer dissolved in an aqueous acid below a pH of 2 [46]. The application of voltage supplies charge that allows the aniline monomer to reduce to a radical cation onto the surface of the electrode in one of the configurations shown in Figure 3 [46][47][48]. Radical cations near the surface couple together and rearrange to a more energetic formation, allowing it to eliminate two protons as shown. This molecule is called p-aminodiphenylamine (PADPA) [49]. The chain can propagate similarly when PADPA connected to the substrate oxidizes and couples with other radical aniline ions [49], [50]. It is possible for a radical cation to react with a neutral aniline monomer when less radicals are available, but it is more energetically favorable to form PADPA as an intermediate [49]. This process will continue to lengthen the end of the chain following the mechanism in Figure 4, but branching and substitution can change the chain shape and properties [50], [51].

Branching occurs when aniline cations attach to the middle of a chain at a nitrogen site and substitution is when the cation R attaches to a ring as shown by the scheme
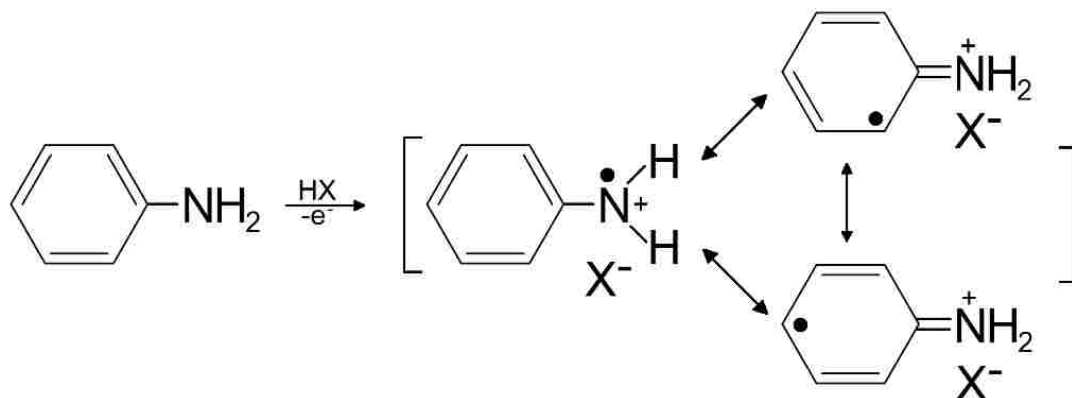
FIG. 3: The cationization of aniline monomer to one of the radical forms.
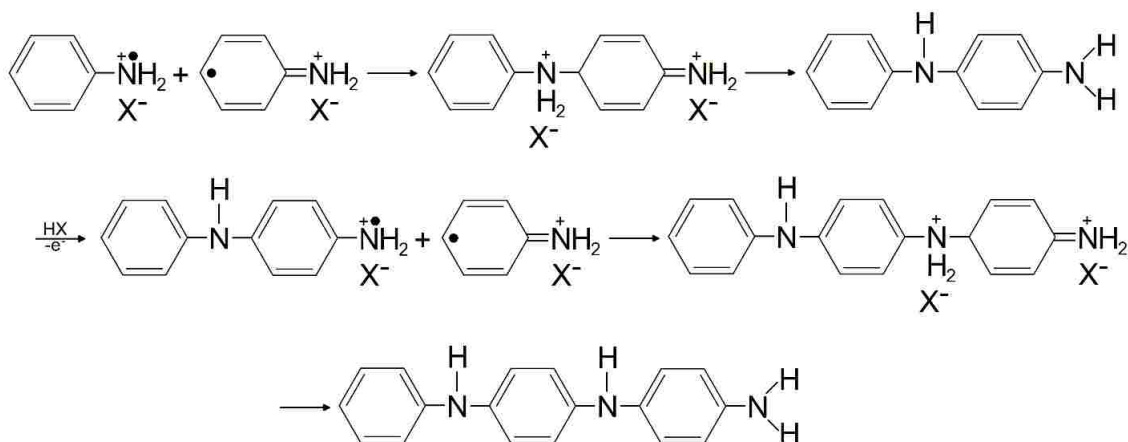
FIG. 4: The growth and propagation mechanism of a polyaniline chain.

in Figure 5 [50], [51]. These growths contribute to crosslinking in polyaniline which can change the overall properties. It has been demonstrated that controlling the amount of branching and substitution can influence the morphology of polyaniline to form nanotubes, microrods, aggregated particles, and sheets [52]. Research has also found that too much crosslinking in polyaniline can inhibit surface reactions in pores due to increased ionic resistivity [53].

1.3 REDOX MECHANISM OF HYDROQUINONE
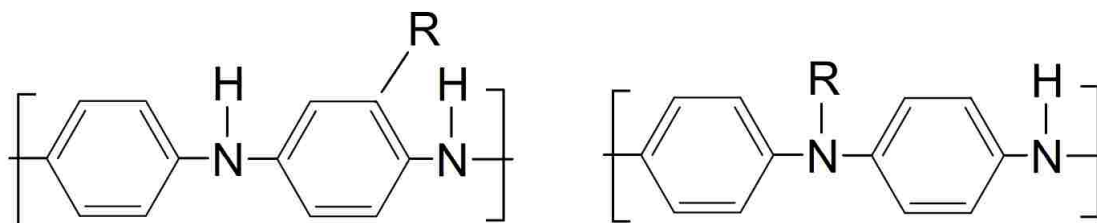
FIG. 5: Branching (left) and substitution (right) mechanisms that can affect the morphology of PANI.

FIG. 6: A hydroquinone molecule diagram
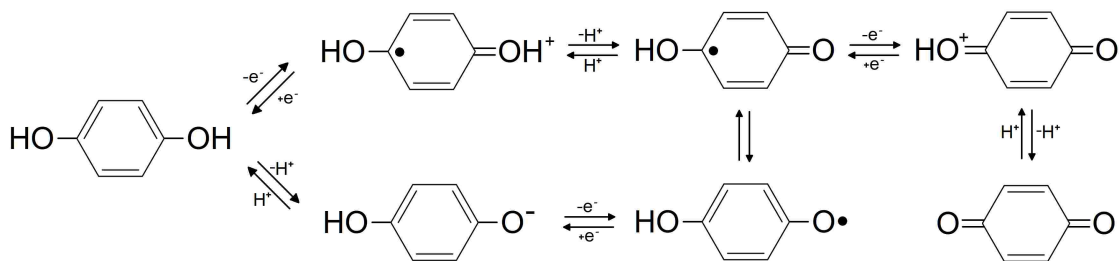
FIG. 7: The redox mechanism of hydroquinone and benzoquinone in a pH of about 0.3. Adapted with permission from Cooper and Hall [54].

Many researchers choose to implement redox mediators into their electrolyte to increase performance. Redox mediators can increase the conductivity of the electrolyte and contribute charge storage by reacting with the surface of the electrode [55]. The specific capacitance is improved without modifying the electrode and can result in devices with energy densities comparable to that of a battery [56]. Some redox mediators even synergize together in the same electrolyte to increase the performance more than each do individually [57].

Hydroquinone is a quinonoid ring with a hydroxy group connected to either end as shown in Figure 6. It is an excellent redox mediator to use for polyaniline supercapacitors due to the low cost and the catalytic effect PANI has on the redox reaction between hydroquinone and benzoquinone [58]. With low enough pH, it can be reversibly oxidized to benzoquinone in a two electron mechanism; the reaction for a pH of 0.3 is depicted in Figure 7 [54].

The reaction begins with the adsorption of hydroquinone at the acid centers of emeraldine salt through the formation of a hydrogen bridge to mediate the charge [59]. This means the oxidation of emeraldine salt in 1M H_2SO_4 must occur first. Also researchers have previously determined that oxidation of leucoemeraldine to emeraldine salt is slower than the oxidation of hydroquinone to benzoquinone, so oxidation of leucoemeraldine to emeraldine salt is the rate determining step of the reaction [58]. After bridging to emeraldine salt and oxidizing to benzoquinone, the two freed electrons are supplied to the imine at the acid center, and subsequently the PANI chain is oxidized to pernigraniline [60]. The reduction process occurs in the reverse order and practically no overpotential is necessary for oxidation or reduction [60].

1.4 MOTIVATION

Commercial supercapacitors are typically made of activated carbon and exhibit

specific capacitance values around 25-30 F g^{-1} with energy density values up to about 6 Wh kg^{-1} [61]. Acetonitrile solvent is generally used in commercial supercapacitors due to its high operating voltage, high conductivity, and low viscosity, but is expensive and dangerous [62]. Manufacturing with organic solvents requires intensive environmental controls, because trace amounts of water can severely reduce the operating voltage [63]. Water as a solvent limits the operating voltage to around 1V due to the decomposition of water at 1.23V. Even with this limitation, researchers have designed PANI supercapacitors using 1M H2SO4 as an electrolyte that can massively outperform commercial devices. Plus water is without a doubt the most environmentally friendly solvent with a fraction of the cost of any other solvent.

PANI can theoretically exhibit a specific capacitance of 2056 F g^{-1} assuming all of the PANI is involved in charge storage [12]. In practice, PANI electrodes were reported to exhibit up to 577 F g^{-1} in 1M H_2SO_4 [52], [64, 65, 66], yet no PANI-based supercapacitors can be found on the market. This can be partially attributed to the high-cost and low throughput of the complicated procedures researchers tend to follow when attempting to fabricate the best possible devices. Researchers have already demonstrated that aniline precursor solution can be recycled [52], but a simple manufacturing process to create safe and environmentally friendly PANI supercapacitors for minimal cost is needed.

Fabricating PANI supercapacitors through electropolymerization does not require expensive equipment and can form films of controlled morphological growth. To be effective, PANI requires a high surface area. Increasing the film thickness or the pore density of the film can dramatically increase the resistance if the material has low conductivity or the electrolyte poorly diffuses through the pores. The work of this thesis investigated the capacitance of PANI films fabricated on stainless steel through electropolymerization based on the growth voltage. The highest capacitance film shows massive improvement with hydroquinone in the electrolyte as a redox mediator.

Symmetric full-cell devices then were first fabricated using this aqueous electrolyte. Then polyvinyl alcohol was added to the electrolyte to form a gel polymer electrolyte, which was used to construct solid state supercapacitors. Polyvinyl alcohol is chosen due to its low cost, ease of manufacturing, non-toxicity, and its hydrophilicity [67]. The solid state design can hurt the performance due to higher resistance, but solid state electrolytes reduce the danger of electrolyte leakage and greatly simplifies cell design [68].

1.5 METHODOLOGY

To form a PANI film through electropolymerization, two identical stainless steel electrodes were placed in a cell with aqueous precursor solution containing aniline and sulfuric acid and voltage is applied. The cell is a box designed with just enough room for 8 mL of solution between the electrodes. A low volume deposition not only keeps the material cost down, but can reduce the space required to manufacture devices. To find out which voltage produces a film with desirable morphology, electropoly-merization was performed incrementally across a range of voltages to find which films exhibited peak specific capacitance. To further improve the performance of the highest performing film, hydroquinone was implemented as a redox mediator. The optimized electrode was then built into supercapacitors with aqueous electrolyte con-taining hydroquinone. Supercapacitors were also fabricated using electrolyte without hydroquinone to verify that hydroquinone contributes to improved performance in a full-cell design. After this was proven to be true, the design was reiterated to include polyvinyl alcohol in the electrolyte as a plasticizer. The electrolyte gel has more utility than liquid electrolytes because it can hold the device together when it dries and can reduce the cost of finishing the cell to be safe.

CHAPTER 2

EXPERIMENTAL

Thin films of polyaniline were electropolymerized onto the surface of stainless steel substrates at voltages from 1.07V to 1.21V to investigate the optimal deposition parameters for the specific precursor solution chosen. The resulting films are electrochemically tested to determine the charge storage capabilities when different films are formed. Once the optimal PANI electrode preparation technique was found, electrodes were fabricated into symmetric hybrid supercapacitors.

The chemicals used in the experiment were used as received from the distributor. All water used in this thesis was deionized (DI). Aniline was kept in a nitrogen glove-box to minimize degradation over time. The substrates were cleaned heavily to remove any grease or dirt that might remain from the machine shop. They were cleaned with acetone twice before cleaning with methanol and isopropyl alcohol.

The precursor solution consisted of DI water, H_2SO_4, and aniline. To ensure accurate measurements of H_2SO_4 and to streamline production, 1M H_2SO_4 was carefully made first. A syringe was used to add a precise amount of H_2SO_4 to DI water that was accurately measured in a volumetric flask. Accurate measurement is important to ensure consistency as this electrolyte solution was used as a basis for electropolymerization as well as the base of the electrolytes used for electrochemical testing. Any error that is made in preparing this solution will propagate through the whole process; however, using this solution for all electrolyte needs can drastically simplify manufacturing. In a typical experiment, the precursor solution was then made from 50 mL of 1M H_2SO_4 added to 75 mL DI water followed by 5.5 mL of aniline added dropwise under constant stirring until homogeneous. The remaining 1M H_2SO_4 solution was used later as an electrolyte for electrochemical characterization.

Electropolymerization was carried out potentiostatically for 3 minutes in a two electrode system with matching stainless steel substrates at room temperature. The electrodes are masked on the back and a strip on the front to act as the contact. Each electrode is made with only 8 mL of solution. After electropolymerization, the substrates are propped up to drain excess solution and dry for three minutes before washing with DI water. The substrates are then dried in a vacuum chamber overnight before characterizing or assembling into a supercapacitor.

2.1 CHARACTERIZATION

The power supply used for electropolymerization in this experiment was a B&K VSP6020. A CorrTest CS150 electrochemical workstation was employed to test the electrochemical performance of full-cell and half-cell devices. For half-cell tests, a Hanna Instruments saturated calomel reference electrode was connected as the reference electrode with a platinum counter electrode. SEM images were collected with a JEOL SEM JSM 6060 LV. A Perkin Elmer Lambda 45 spectrophotometer was used to collect UV-VIS measurements.

2.1.1 CYCLIC VOLTAMMETRY

Cyclic voltammetry (CV) is a powerful electrochemical characterization technique in which voltage is scanned across a range at a certain scan rate and the current response is analyzed. This technique is used often to determine the electrochemical performance of supercapacitor electrodes in a half-cell three probe system or a complete supercapacitor device in two probe configuration; however, it can also be a valuable technique for material synthesis, approximating surface area [69], or investigating the bandgap structure [70]. For supercapacitors, the current response curve can be analyzed to find the capacitance, the energy density, the power density, and the contributions due to EDL or redox mechanisms.
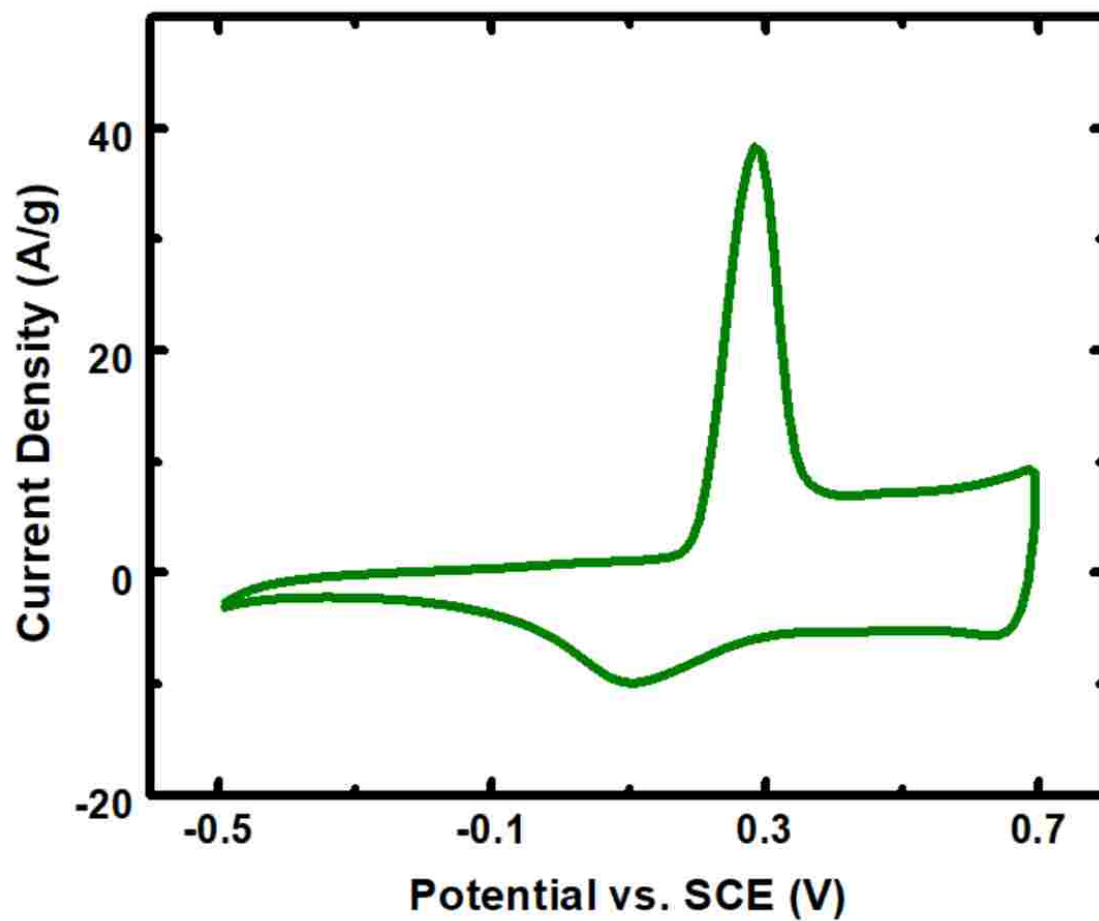
FIG. 8: Voltammogram showing the current response of a PANI film as the voltage is scanned between -0.5V and 0.7V.

Figure 6 shows the cyclic voltammogram recorded for a random PANI electrode. The current response curve depicts the charge storage and discharge over time. The top curve is the charge response when the voltage is swept from -0.5V to 0.7V and bottom curve is the discharge current as the potential is swept back to -0.5V. The gradual curve shape can be attributed to EDL capacitance mechanisms or pseudo-capacitance while sharper peaks are resultant of other redox mechanisms that arise at specific potentials. A system in which each molecule transfers n electrons exhibits ideal behavior when the distance between the oxidation and reduction peaks is 58/n mV (at 25°C) [71]. The actual peak-to-peak separation is related to the reaction rate, where the peaks separate and broaden when the system isnt able to keep up. This can be a result of slow reaction kinetics or lack of electrolyte diffusion into the porous electrode [72]. The reaction rate must be fast enough to fully charge and discharge within the operating voltage window at a given scan rate or not all active sites will contribute to the energy storage mechanisms.

The overall capacitance C for supercapacitor in a half-cell is the total amount of charge transfer ΔQ_{total} that occurs during charging and discharging across the voltage window ΔV [73]:

$$C = \frac{\Delta Q_{total}}{2\Delta V} \tag{10}$$

The total charge in the system ΔQ_{total} is the full area between the charging and discharging curves of the cyclic voltammogram, but can be roughly broken down into the charge accumulated C_1 from the area under the charging curve and the charge discharged C_2 from the area under the discharge curve. The charging capacitance C_1 can be calculated from the cyclic voltammogram from the charge accumulated Q_1 across the voltage window ΔV [74]:

$$C_1 = \frac{\Delta Q_1}{\Delta V} \tag{11}$$

In this case, the total charge gained ΔQ_1 is the area under the charge response curve $I_1(V)$ at a given scan rate v:

$$\Delta Q_1 = \frac{1}{v} \int_{V_{min}}^{V^{max}} I_1(V)dV \tag{12}$$

This results in a charging capacitance [72], [74]:

$$C_1 = \frac{1}{v\Delta V} \int_{V_{min}}^{V^{max}} I_1(V)dV \tag{13}$$

Likewise, the discharge response curve $I_2(V)$ can be integrated to find the charge discharged ΔQ_2. While numerical integration can be used to easily find the total area between the curves, the charges can be found and plugged into equation 16 to determine the overall capacitance of the device. The charges can also give insight to the coulombic efficiency by comparing the charge discharged to the amount of charge that accumulated while charging, but the columbic efficiency is typically found through the galvanostatic charge/discharge that will be discussed next [76].

The capacitance in a two probe full-cell system, generally a fully constructed supercapacitor device, can be found using the same equations as a three probe system, but the specific capacitance is adjusted with a 4x multiplier to account for the mass of two electrodes [77].

2.1.2 GALVANOSTATIC CHARGE-DISCHARGE

Energy storage mechanics can be investigated by studying the response to various forms of electrical input: applying constant current, sweeping voltage at a certain scan rate, or alternating current at a range of frequencies [78]. The first way is the mechanic that drives galvanostatic charge-discharge (GCD), while the second of these

is obviously the basis behind cyclic voltammetry. The third way is incorporated into the technique known as electrochemical impedance spectroscopy.

Galvanostatic charge-discharge, also called constant current charge-discharge or chronopotentiometry, is the application of constant current density to study the potential response as it charges to a specified voltage and discharges. This technique is the best method for evaluating the actual performance of a fully fabricated device, and it is considered to be the most useful supercapacitor characterization technique when it comes to versatility and accuracy [11], [79]. Similar to the cyclic voltammogram response curve, the ideal response of EDL charge storage mechanics and actual pseudocapacitance is linear and symmetric, while most redox active materials exhibit nonlinear response curves as reactions occur quickly corresponding to certain voltages [80], [81].

Observe Figure 9a depicting the shape of an ideal potential response curve for a supercapacitor in pink [82]. The area under the curve is related to the capacitance of a half-cell by [77], [83]:

$$C = \frac{I}{dV/dt} = \frac{I\Delta t}{\Delta V} = \frac{I\Delta t}{V_{max} - V_{min}} \tag{14}$$

The device is discharged with constant current I once it reaches V_{max} and takes an amount of time Δt to reach V_{min}. A linear discharge curve will have the characteristic slope dV/dt. Nonlinear plots of more battery-like devices can be integrated over the area instead [2]; however, charge discharged at a constant discharge current will be the same over a given interval of time regardless of the shape of the potential response, so the capacitance can still be derived just from the discharge time, current, and operating voltage. This formula is similar to the capacitance formula for cyclic voltammetry, with the difference being that the GCD curve can be easily broken into charging and discharging. Obviously, the important capacitance is the discharge

capacitance that the device will actually output for energy storage purposes, but other details can be drawn from the potential response.

Assuming the device is not perfect, there is an initial voltage drop that occurs when the device begins to discharge that is related to the internal resistance of the device R [84]:

$$R = \frac{V_{drop}}{2I} \tag{15}$$

This is depicted in Figure 9b as indicated where the voltage quickly drops and then becomes linear shortly after [82]. Leakage current can also be present in a supercapacitor. A supercapacitor with low leakage current will be practically linear and symmetric as shown by the pink line in Figure 9a, but the blue line represents a device with more leakage current [82].

The coulombic efficiency η is accurately determined from GCD measurements by comparing the amount of time it takes to discharge t_D with the time it takes to charge t_C [85]:

$$\eta = \frac{t_D}{t_C} * 100\% \tag{16}$$

To compare the specific capacitance values with those run in a full-cell test, a factor of four has been used as a multiplier for GCD measurements as well [86], [87].

2.1.3 FOURIER TRANSFORM INFRARED SPECTROSCOPY

The atoms within a molecule above absolute zero constantly vibrate, in which the bonds stretch or bend at a natural frequency [88]. This phenomenon can be roughly modeled similar to Hookes law with balls connected by springs to represent the atoms and bonds [89]. Physically, photons are absorbed to increase vibrational energy when their frequency matches the natural vibrational frequencies of bonds within
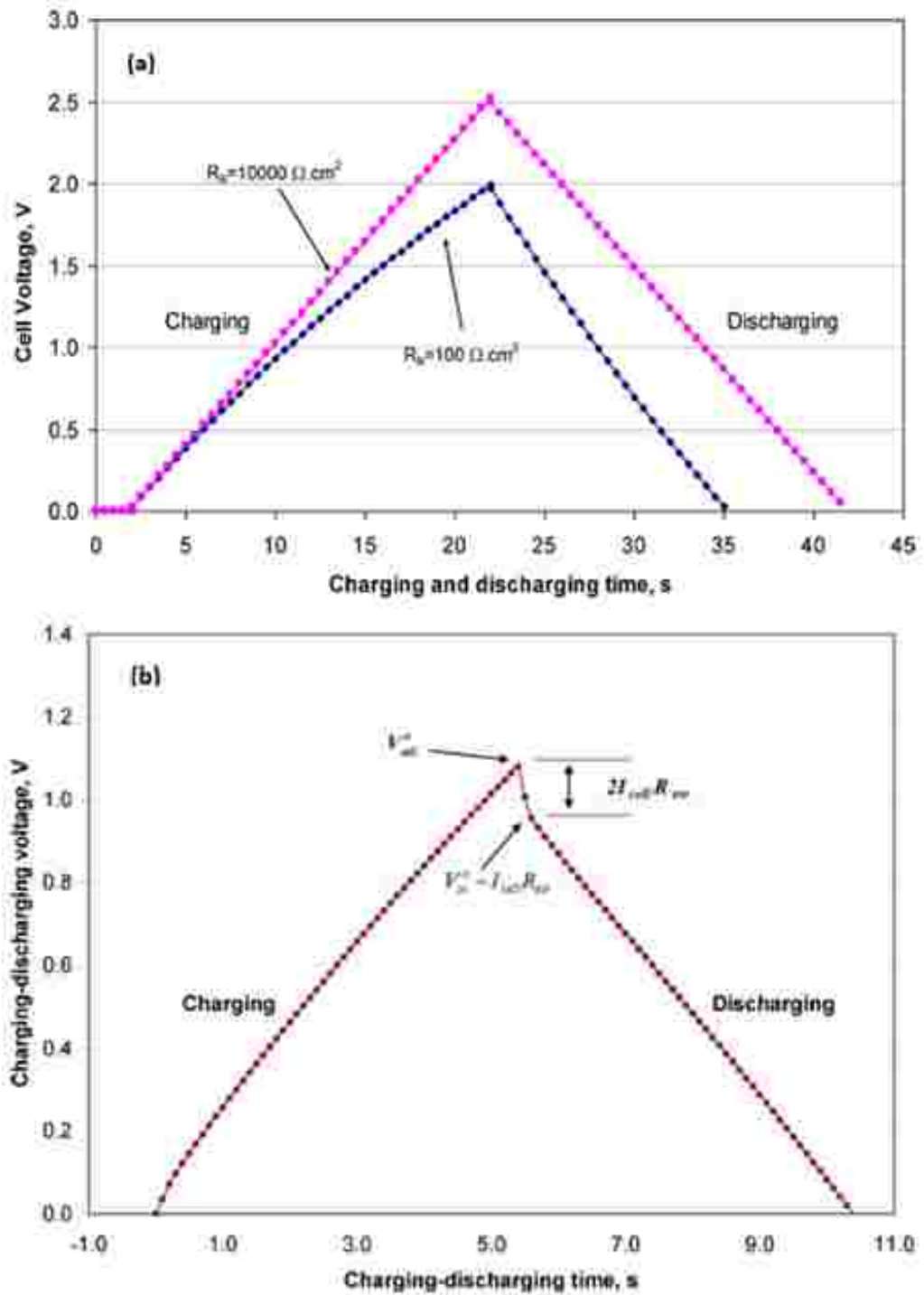
FIG. 9: Depictions of non-ideal behavior influencing device performance. a) Leakage current and b) internal resistance. Reproduced with permission from Ban, et al. [82].

the molecule, which occurs in the infrared region [88]. Fourier-transform infrared spectroscopy (FTIR) is a technique that utilizes this phenomenon to characterize materials based on the energies they absorb by corresponding the values with the known values of specific bonds [89]. This can be especially useful for polymer analysis as these bonds can give details of the molecular structure and the identification of functional groups can help distinguish between similar compounds [89].

2.1.4 ULTRAVIOLET-VISIBLE ABSORPTION

Ultraviolet-visible (UV-VIS) absorption is a technique in which light in the ultraviolet and visible wavelength range is shined through a film to determine which energy bands of light are absorbed and which pass through. This can give details of the molecular orbital structure as photons in the visible and UV range are absorbed by bandgaps of similar energy [88]. Vague physical conclusions of what bonds are present can be drawn based on the peaks and valleys of the absorption curve. Assessments made by UV-VIS can be strengthened by pairing this technique with other physical characterization techniques, such as FTIR.

2.1.5 SCANNING ELECTRON MICROSCOPY

A scanning electron microscope (SEM) is one of the most common techniques for capturing a high resolution image of a sample. It scans discrete locations over an area by firing electrons at each location and mapping electrons that are detected from backscattering and secondary electron generation [90]. Where optical microscopes have limited resolution due to the wavelength of visible light, electrons ejected with an energy of 10 kV are found to have a wavelength of 0.012 nm [91]. This allows much higher resolution, but ushers a new requirement that the sample must be electrically conductive in order to receive and eject electrons. To map the surface of a non-conductive surface, simply coat the film in a thin layer of gold. Observe Figure 10,
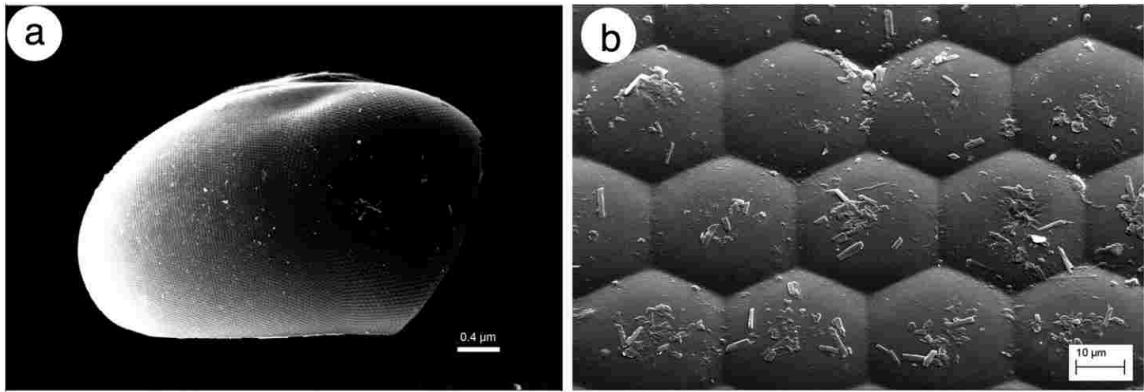
FIG. 10: A dragonfly eye imaged using SEM. Reproduced with permission from Kaya, et al. [92].

an image taken of a dragonfly eye using SEM shows the mineral growth on the surface of the eye [92].

CHAPTER 3

POLYANILINE THIN FILM ELECTRODES

The concentrations of aniline and sulfuric acid in the precursor solution along with the voltage applied to the cell will influence the growth behavior of the polyaniline film. Voltages from 1.07V to 1.29V were employed for a deposition time of three minutes to study the effect of voltage on the deposit. Then the optimized electropolymerization process was varied with the time parameter to ensure the chosen process yields growth that was the most electrochemically active.

It was found that allowing the films to dry for more than three minutes before washing caused the darker bulk on top to adhere to the thin film more. Thick polyaniline layers can be highly resistive and hold on to excess monomer. Results were kept consistent by shaking the electrode in DI water, after drying for three minutes, to remove bulk deposits and loose particulates.

3.1 CHANGE IN ELECTROPOLYMERIZATION VOLTAGE

The change in voltage from 1.07V to 1.29V exhibited extreme changes in color as shown in Figure 11. This demonstrates the high level of voltage dependence on the polymer formation. The morphology will be discussed in more detail from
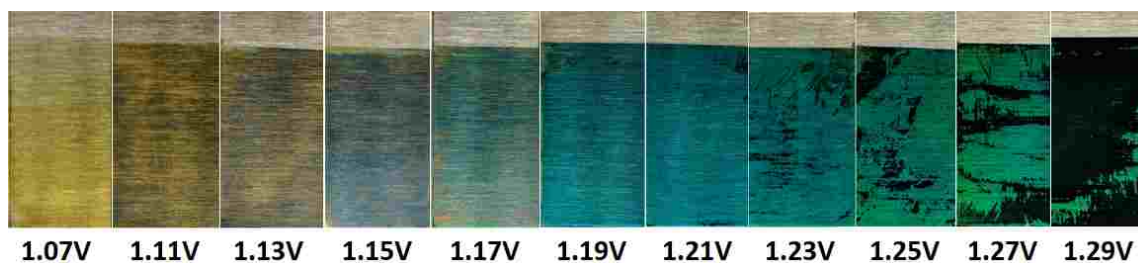
FIG. 11: Electrochromic colors of electrodes fabricated with increasing voltage

characterization data, but some obvious differences can be observed even with the naked eye due to electrochromism. At low voltage, a yellow film is formed. As the voltage is raised, there is further oxidation to turn the film blue then green with dark green bulk. Excessive bulk growth that will not wash off easily occurs more as the voltage is raised. The electrochemical implications of these different films will be discussed along with limited physical characterization.

3.2 ELECTROCHEMICAL CHARACTERIZATION

Cyclic voltammetry in a half cell with three electrodes was the primary technique used to compare film performance as energy storage characteristics are ultimately the most important for supercapacitors. The electrodes were tested from 0v to 0.8V vs saturated calomel electrode (SCE) in 1M H_2SO_4 aqueous electrolyte. The scan rate was usually set at 100 mV/s to compare samples and can be assumed to be such unless otherwise stated.

Specific capacitance is regarded as one of the most important characteristics to maximize for supercapacitor design. The specific capacitance for samples made at 1.21V was the highest on average with 612 F/g. The rest of the results are compared in Figure 12. The polyaniline film made at 1.07V is the least performing of all with 154 F/g, but the specific capacitance of the films gradually increases as the voltage is raised to 1.21V. Around 1.21-1.23V, the performance plateaus and begins to decrease. At 1.29V the film is very thick and exhibits only 265 F/g. The reason for this performance can be more understood by comparing the cyclic voltammograms from three samples produced at 1.07V, 1.21V, and 1.29V shown in Figure 13. They will be referenced as PANI(1.07V), PANI(1.21V), and PANI(1.29V).

For PANI(1.21V), the potentials that the peaks occur at agree with well-documented values [26], [32], [93, 94, 95]. The charging peak at ∼0.21V occurs when the film oxidizes to the emeraldine state. The peak that occurs at ∼0.76V

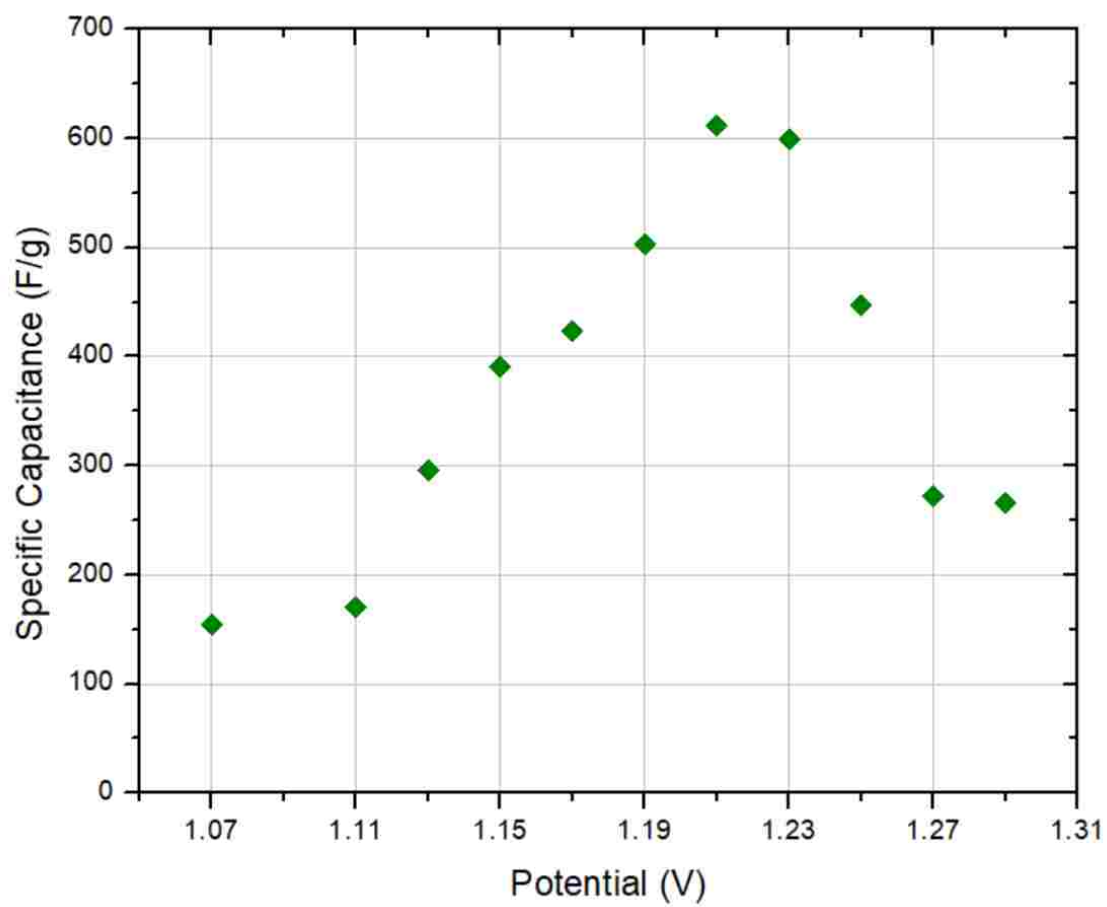FIG. 12: The change in specific capacitance as electropolymerization potential is varied for PANI films tested in a half-cell at 100 mV/s.
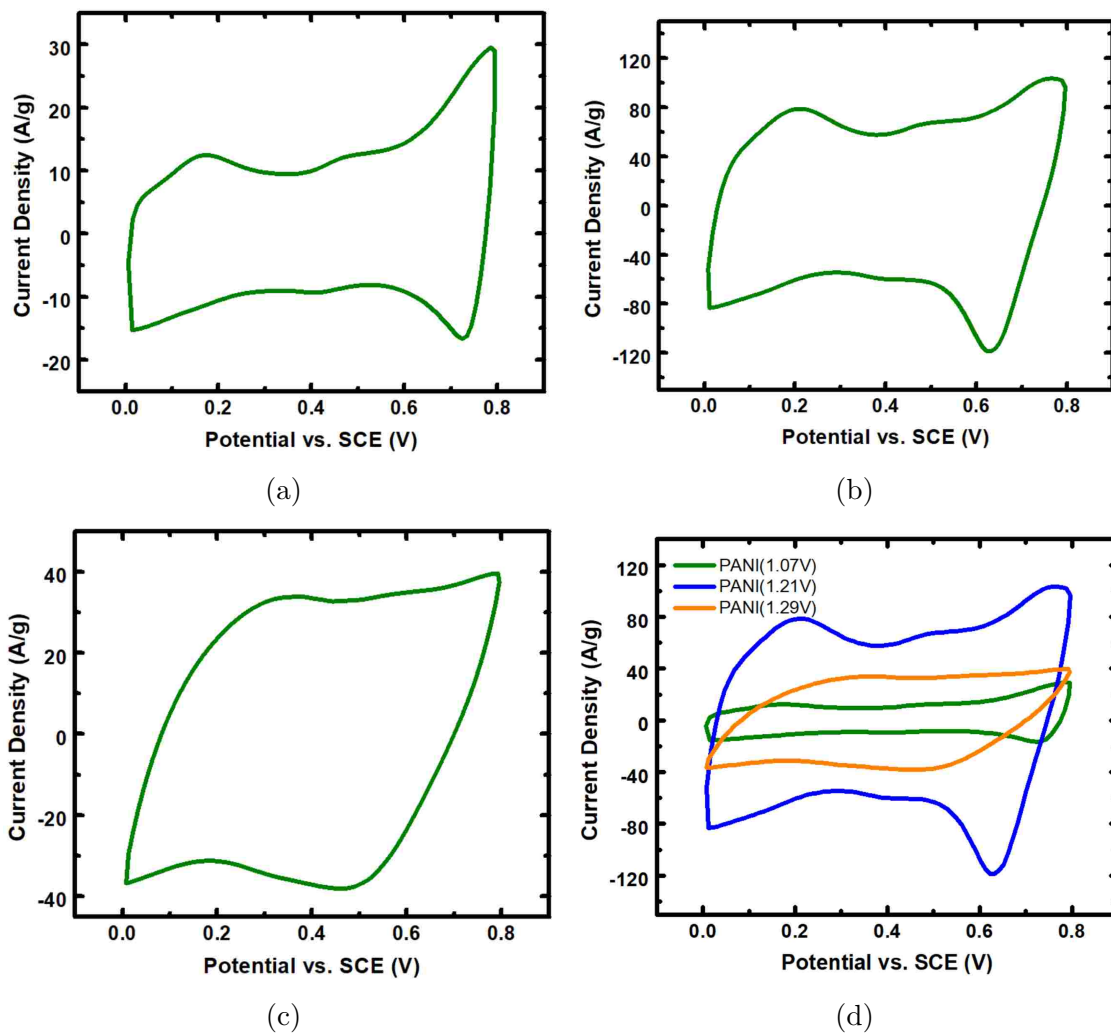
FIG. 13: The current response curves in a half-cell at 100 mV/s for polyaniline electrodes fabricated at: a)1.07V, b) 1.21V, and c) 1.29V. d) The three plotted together for comparison.

results from the polyaniline oxidizing to the pernigraniline state. On the discharge curve, a peak at ∼0.63V appears as the pernigraniline film is reduced back to emeraldine. Another peak that is out of range (∼-0.2V) is the resulting charge transfer from slowly reducing the emeraldine state down towards the leucoemeraldine region. An extra pair of peaks can occur between those transitions from redox mechanisms of quinonoid defects transitioning between hydroquinone to benzoquinone [96], [97]. This defect peak is minimal, indicating there are few quinonoid defects present in the sample. The average weight of the films prepared at 1.21V is about 150 micrograms.

The electrode that was electropolymerized at 1.07V produced a thin yellow polyaniline film. The same peaks are present for oxidation and reduction, but much less charge is passed. Additionally the transition from leucoemeraldine to emeraldine occurs at a lower potential when compared to PANI(1.21V). This suggests that the reaction kinetics are faster, which could be from fewer active redox sites in PANI(1.07V). As will be discussed with the SEM results, the polyaniline film made at 1.07V has much less surface area due to its planar morphology. Faster reaction kinetics could also result from lower ionic resistance as the electrolyte easily interfaces the entire surface of the electrode. The average weight for the films prepared at 1.07V is about 100 micrograms.

The thick polyaniline film fabricated at 1.29V exhibits resistive behavior that gives it a pseudocapacitive effect. The oxidation peak where leucoemeraldine transitions to emeraldine is shifted at least 0.1V with extensive peak broadening. The same can be observed for the reduction peak from pernigraniline back to emeraldine. The oxidation peak for the pernigraniline transition is shifted out of the operating range, but an increase in current can be seen as the reaction begins. For all samples, the full transitions to leucoemeraldine and pernigraniline are out of the operating range, but PANI(1.21V) is able to achieve peak current from the transition to pernigraniline. The average weight for the films prepared at 1.29V is about 800 micrograms.
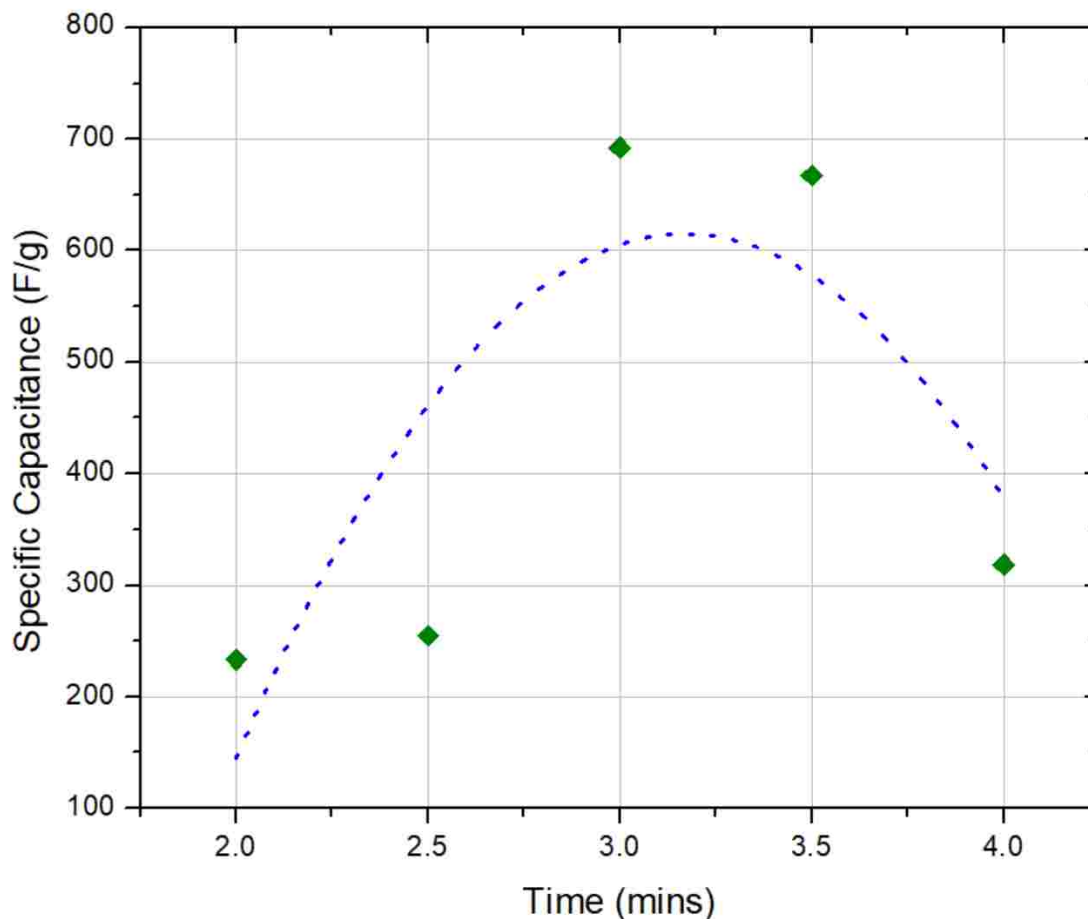
FIG. 14: The effect of changing the deposition time when fabricating PANI(1.21V).

PANI(1.29V) actually stores more than three times the energy compared to PANI(1.21V), but PANI(1.29V) has a much lower specific capacitance since it also weighs more than five times as much. When these are plotted together with the same test, the areas can be compared to determine which stores more charge. Figure 13d shows the CV curves for PANI(1.07V), PANI(1.21V), and PANI(1.29V) together, which clearly shows a much higher specific capacitance for PANI(1.21V) based on the area of the curve.

Electropolymerization has an edge over chemical oxidation since the polymerization process can be abruptly started and stopped by simply turning the power
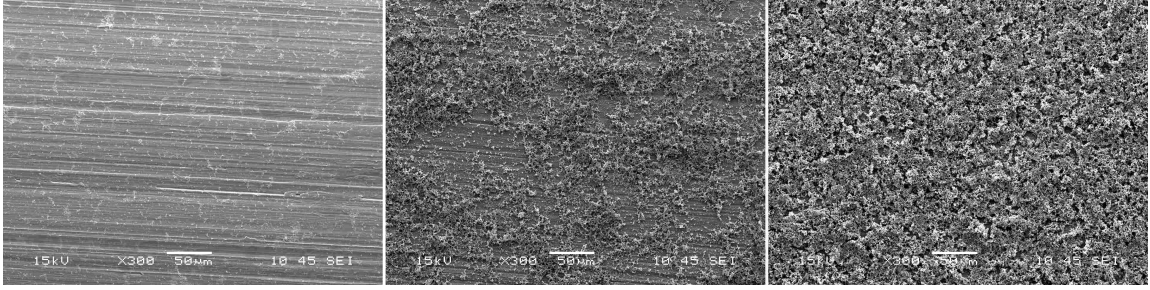
FIG. 15: The general morphology of PANI(1.07V), PANI(1.21V), and PANI(1.29V) respectively as seen by an SEM at a magnification of only 300x.

on or off. Changing the electropolymerization time for this experiment influenced what stage of growth the film is in. The potential that produced the highest capacitance films was also fabricated utilizing different electropolymerization times to determine if stopping its growth earlier or allowing it to grow further will increase the electrochemical capability of the film. The average specific capacitance for each polymerization time attempted can be observed in Figure 14. It was found that even reducing the deposition time by 30 seconds was enough to drop the specific capacitance to about 250 F/g as the film was underdeveloped. Further reducing the time lowered the performance slightly more. Adding 30 seconds to the deposition time resulted in electrodes with similar performance to those fabricated with an electropolymerization time of 3 minutes, but above that the capacitance plummeted and the behavior became more resistive. From the data, 3 minutes was the best electropolymerization time for this process, but slight deviations of a few seconds could be investigated with equipment that would allow more control over the experimental conditions. A second order polynomial trendline was fit to the data to give a rough estimate of the best deposition time, which was found to be about 3. Therefore, the optimal processing time was kept at 3 minutes.

3.3 PHYSICAL CHARACTERIZATION

FIG. 16: PANI(1.07V) imaged by SEM under a magnification of x2,500, x5,000, and x15,000 respectively shows slight chain growth scattered on surface.

PANI(1.07), PANI(1.21V), and PANI(1.29V) were investigated using SEM to assess the morphology. Figure 15 shows the general structure of the three films under x300 magnification. The parallel lines that can be seen underneath the film are from the brushed stainless steel substrate. Compared to the three films, PANI(1.07V) is fairly smooth and PANI(1.29V) in covered in thick porous growth. PANI(1.21V) has areas of thick growth with large open areas. A higher magnification is required to study the growth of these films more effectively.

First look at PANI(1.07V) under magnifications of x2,500, x5,000, and x15,000 as depicted in Figure 16. The overall morphology is planar and the film has a yellow color. There are pinhole pores that can be seen in some regions and there are small islands of chain growth. This type of structure has a low specific surface area and there is little ionic resistance from ions penetrating through pores.

The thicker areas of polyaniline growth in PANI(1.21V) was observed at x1,500, x5,000, and x10,000 to better understand the pore distribution, as shown in Figure 17. There is a large variance in pore size as the film thickens. From a magnification of x1,500, pores up to about 10 m can be seen. The pores in the thicker areas are more easily observed with the higher magnifications in Figure 17. There are many micrometer sized pores distributed all over the growth. Smaller pores on the nanometer scale are also apparent. This pore structure evolves from the variety of
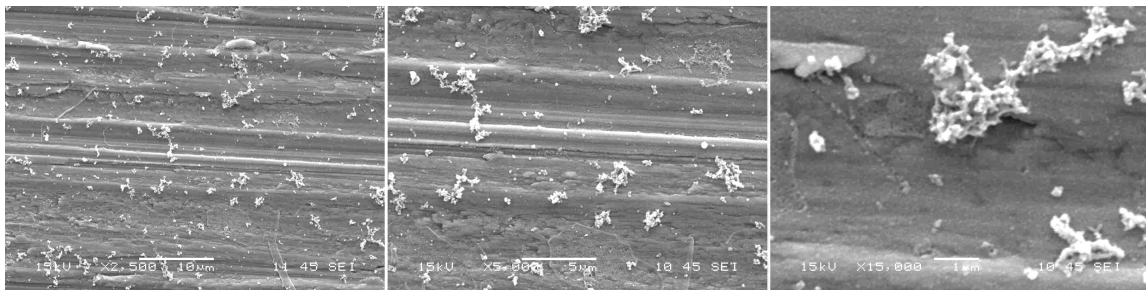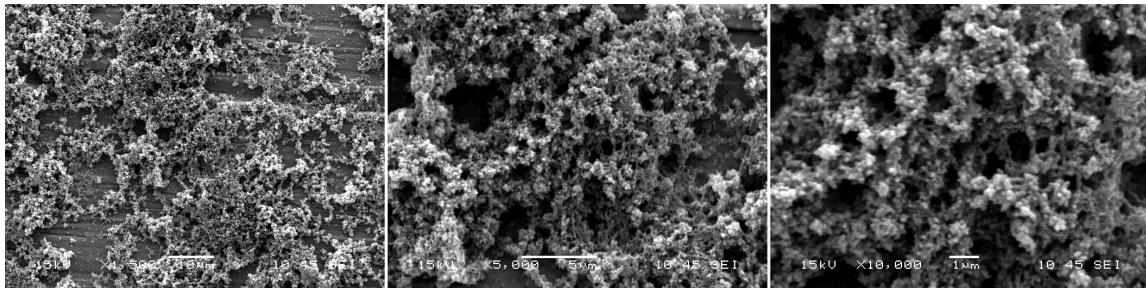
FIG. 17: PANI(1.21V) imaged by SEM under a magnification of x2,500, x5,000, and x15,000 respectively shows slight chain growth scattered on surface.

morphological growth in the film, which is presumably due to changes in concentration and resistance during growth. From the figures, there seems to be granular morphology.

The areas with less growth on PANI(1.21V) were also studied with a magnification of x20,000 to get a better look at the details. The image is shown in Figure 18. Small granular nodes of polyaniline between ∼100 nm and ∼500 nm can be identified. At this magnification the details are blurry, but it is expected that these granules have nanofeatures. Smaller granules, under 100 nm, seem to also be present in areas between larger grains and on larger grains.

The overgrown PANI(1.29V) was observed with SEM under magnifications of x2,000, x5,000, x10,000, and x15,000 as shown in Figures 19 and 20. The overall morphological features of this film are similar to the dense areas on PANI(1.21V). The major difference between these two films is that the entire film is covered in dense growth with very few areas of little growth. A diverse pore distribution can be seen in Figure 19, with some pores on the order of tens of micrometers. Upon magnification, the only discernable difference between the morphology of PANI(1.21V) and PANI(1.29V) is the amount of growth. This thicker porous film causes excessive ionic resistance as the electrolyte ions penetrate through it, which results in a pseudocapacitive effect from peak broadening. Considering this is the case with
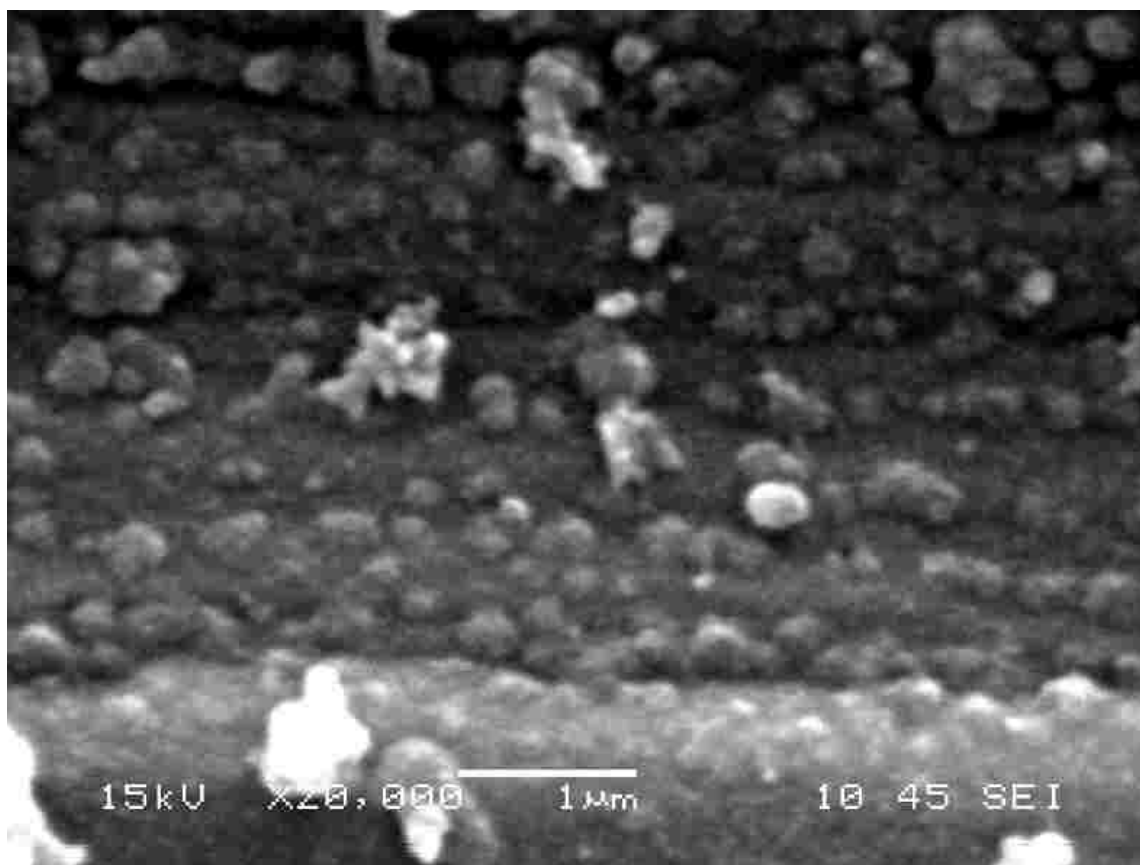
FIG. 18: The barer spots of PANI(1.21V) at x20,000 magnification.
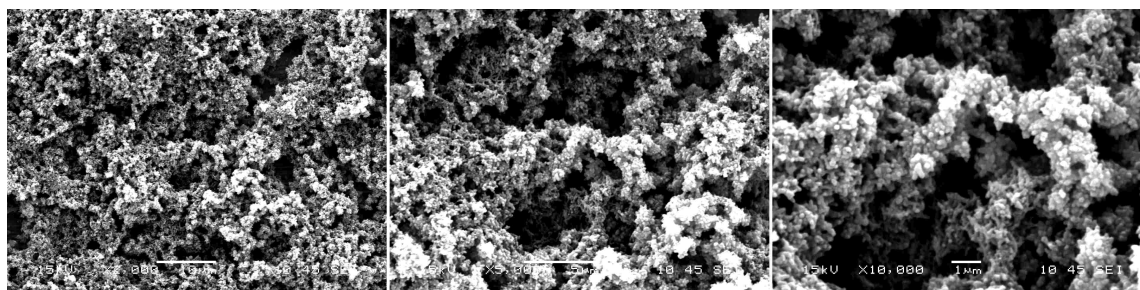
FIG. 19: The SEM images of PANI(1.29V) at magnifications of x2,000, x5,000, and x10,000 show thick growth similar to that of PANI(1.21V).
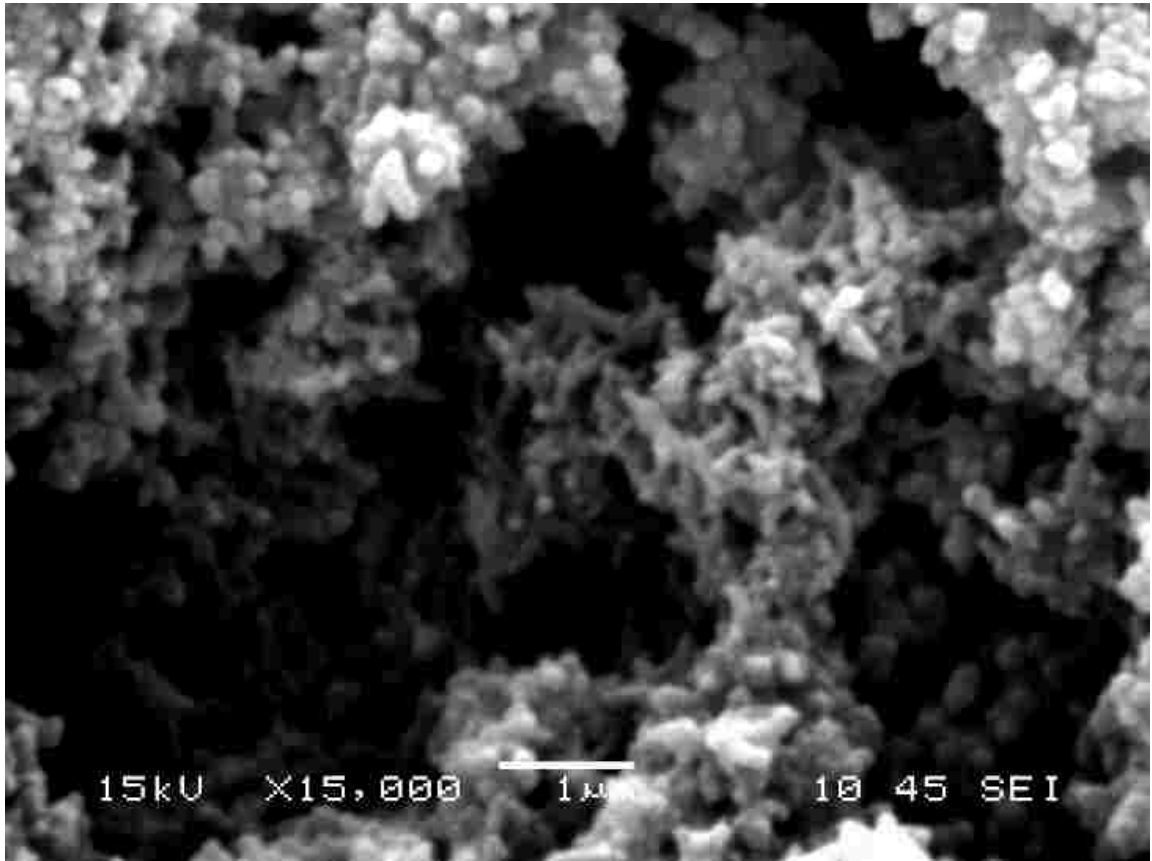
FIG. 20: A high magnification (x15,000) SEM image showing different types of growth.
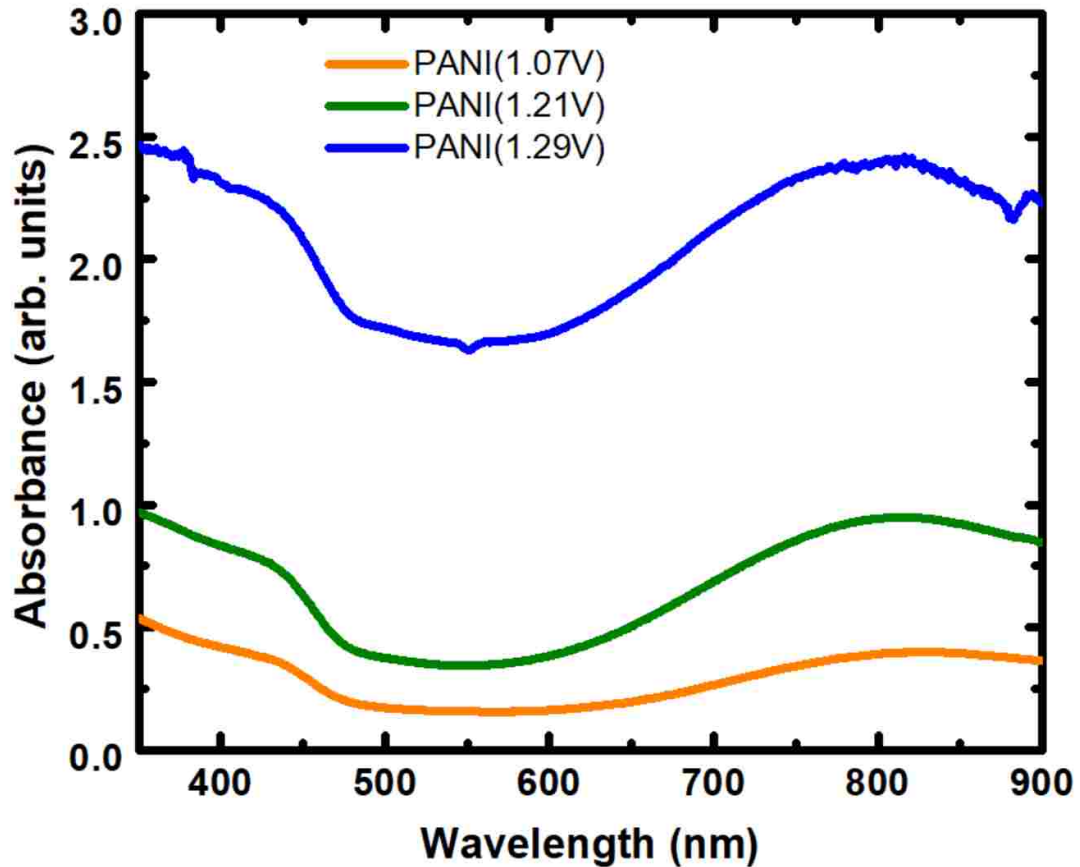
FIG. 21: UV-VIS absorption of PANI(1.07V), PANI(1.21V), and PANI(1.29V) over a range of 350 nm to 900 nm.

aqueous electrolyte and most commercial devices are made with more viscous organic electrolytes, PANI(1.29V) is not a good option for supercapacitors.

UV-VIS absorption was used to further characterize the oxidation state of the films. Figure 21 shows the absorption spectra for PANI(1.07V), PANI(1.21V), and PANI(1.29). Two peaks are visible in the image that both represent absorption in quinonoid rings [99]. The peak that is shown to grow and blue-shift from 830 nm for PANI(1.07V) to 796 nm for PANI(1.29V) corresponds to π-polaron transition [100]. This peak can indicate the level of oxidation in the sample as increasing oxidation increases the intensity of this peak [101]. Also the location of the π-polaron transition
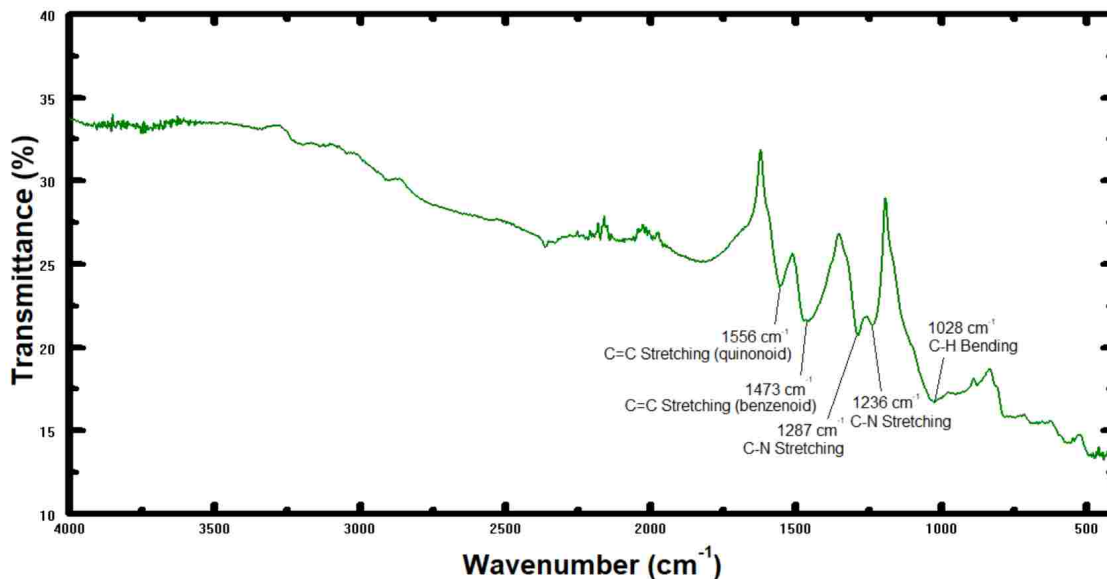
FIG. 22: The FTIR spectra measured for polyaniline on stainless steel.

peak is located around 800 nm for the salt forms and 600 nm for base, indicating the salt forms of polyaniline were formed [102], [103]. The other peak represents polaron-π^* transition and occurs around 435-440 nm in all samples [100]. The edge of a third peak can be seen on the left edge that results from π-π^* electron transition within benzenoid rings [99]. Overall the curve shifts to higher levels of absorbance because the film is thicker when grown at higher potentials.

FTIR was employed to analyze the bond formation of the electrode to verify that it is of the salt form. The results of FTIR confirm peaks at characteristic positions for polyaniline salt as can be seen in Figure 22. The peaks located at 1556 and 1473 cm^{-1} are attributed to C=C stretching of the quinonoid and benzenoid rings [104], [105]. The bands at 1287 and 1236 cm^{-1} can be identified as the vibrational bands of C-N stretching in polyaniline salt [105]. Bending of C-H bonds from sulfate ions in polyaniline salt is assumed to be responsible for the peaks at and under 1028 cm^{-1} [102], [105], [106].

CHAPTER 4

POLYANILINE SUPERCAPACITORS

The next phase of this thesis involved constructing supercapacitors out of optimized electrodes. This portion is focused more on preparation techniques and testing the supercapacitors for actual device performance. Cyclic voltammetry in a half-cell is useful for optimizing a single electrode and testing electrolytes, but building a full cell and testing it with both cyclic voltammetry and galvanostatic charge/discharge will assess real device performance.

First the electrolyte was tested in a half-cell configuration to determine the optimal concentration of hydroquinone (HQ) as a redox mediator. Upon finding this concentration, the electrolyte was tested for real device performance in a full-cell. First, devices were built with the standard 1M H_2SO_4 electrolyte and with the electrolyte containing hydroquinone. Then the final configuration was fabricated, which features a PVA-H_2SO_4-HQ electrolyte to form a solid state device. The solid state electrolyte simplifies device design and can reduce the danger of electrolyte leakage [68].

4.1 ELECTROLYTE PREPARATION

Electrolyte containing various concentrations of hydroquinone were tested in a half-cell by adding the appropriate concentration of hydroquinone to 1M H_2SO_4. The best concentration was used to test the device performance in a full-cell.

Gel polymer electrolyte was employed to build the solid state supercapacitors. Polyvinyl alcohol (PVA) is slowly added to 1M H_2SO_4 in a weight to volume ratio of 10% g/mL and stirred at 50°C for two hours. If the solution did not turn clear, the temperature was raised by 10°C every hour until it did. The temperature was
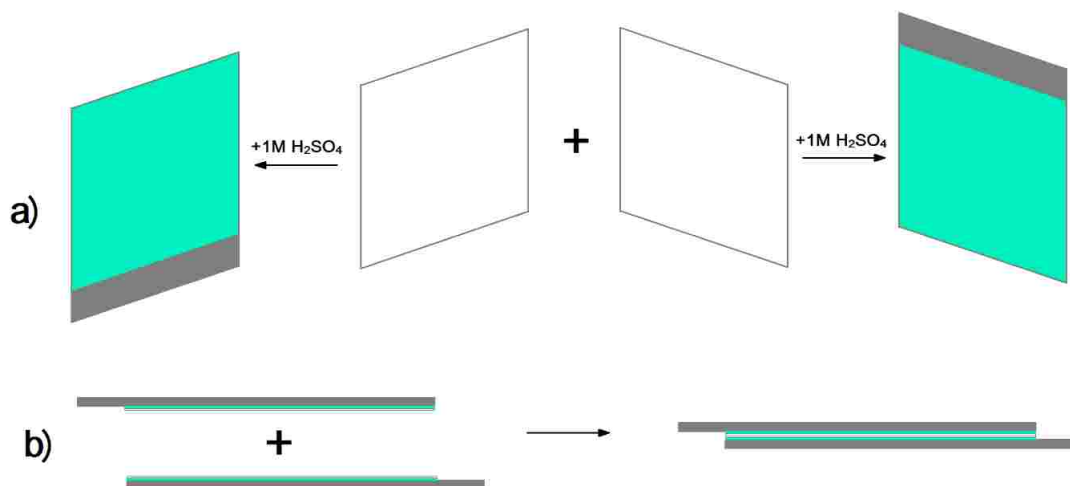
FIG. 23: Diagrams showing how the device is assembled from a) a 3D view and b) a side view.

not raised above 80°C. The redox active gel polymer electrolyte for this project was made with hydroquinone in it by adding the polyvinyl alcohol to 1M H_2SO_4 electrolyte containing hydroquinone.

4.2 DEVICE FABRICATION

The full-cell supercapacitor devices are constructed with a sandwich-like architecture. The liquid electrolyte cells were formed by placing a Kimwipe® cut into a separator onto each electrode, then dropping the electrolyte onto the Kimwipe® to fully wet the electrodes. The electrode faces are then placed together with the contacts on opposite sides as shown in Figure 23.

Solid state devices were also built in the typical sandwich style, but the assembly with the PVA electrolyte was a little different. The PVA electrolyte was painted onto the surface of both electrodes with a watercolour paintbrush, making sure to be careful that the bristles never touch the PANI film. This was left to dry for an hour in the fume hood, then another coat was applied. After another hour of drying, a small

amount of PVA electrolyte was dabbed onto one electrode and the two electrodes were pressed together. This type of electrolyte dries to form a film that can replace the need of a separator [68], [86], [107].

4.3 ELECTROCHEMICAL PERFORMANCE

The first part of the device testing phase was to test the specific capacitance of electrodes in a half-cell with 1M H_2SO_4 followed by testing the electrodes with increasing concentrations of hydroquinone in the electrolyte. The average specific capacitance was initially tested to be about 690 F/g in the standard electrolyte. The electrodes were next tested with 0.1M hydroquinone in the electrolyte. The addition of 0.1M hydroquinone greatly improved the performance to exhibit about 3,416 F/g on average. This is an improvement of almost 5x the performance, proving the intense synergistic behavior between polyaniline and hydroquinone. The electrodes did not show much improvement when the concentration was changed to 0.2M, and the cyclic voltammograms indicated poor cycling behavior based on the shape. The average specific capacitance was about 3,488 F/g for this concentration. A third concentration of 0.3M was attempted, but was found to synthesize large crystals with non-reversible behavior. No data was collected for this concentration as non-reversible behavior is undesirable for supercapacitors. The cyclic voltammograms for an average performing electrode with each of the concentrations tested are shown in Figure 24. Since both the 0.1M and 0.2M solutions have about the same performance, the electrolyte with 0.1M was chosen as the best concentration for this device. This is in part because the concentration of hydroquinone has an effect on the ionic conductivity of the electrolyte, and it was determined that the highest conductivity of a PVA-H_2SO_4 gel polymer electrolyte with hydroquinone had a concentration of 0.1M [108].

The next step was to test these devices in a full-cell with the standard electrolyte
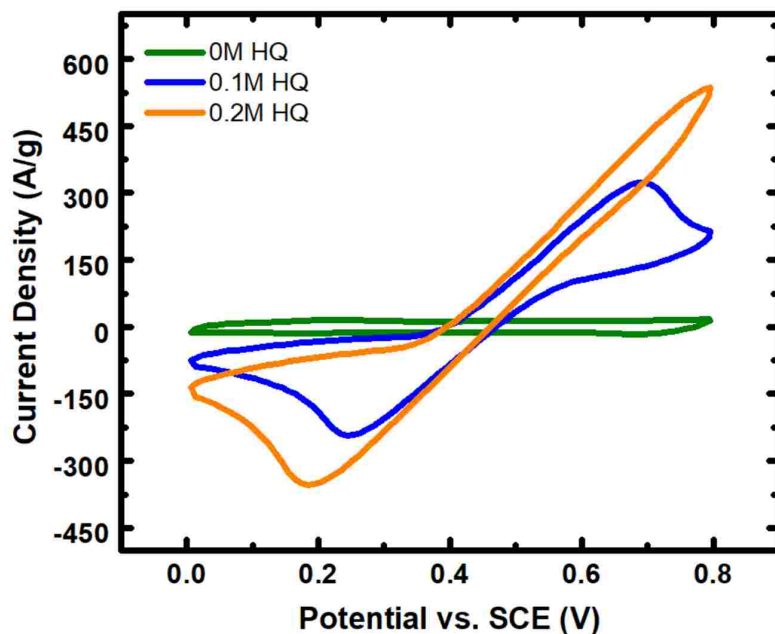
FIG. 24: Cyclic voltammograms of PANI(1.21V) in a half-cell at 100mV/s when hydroquinone is added to the electrolyte in different concentrations.
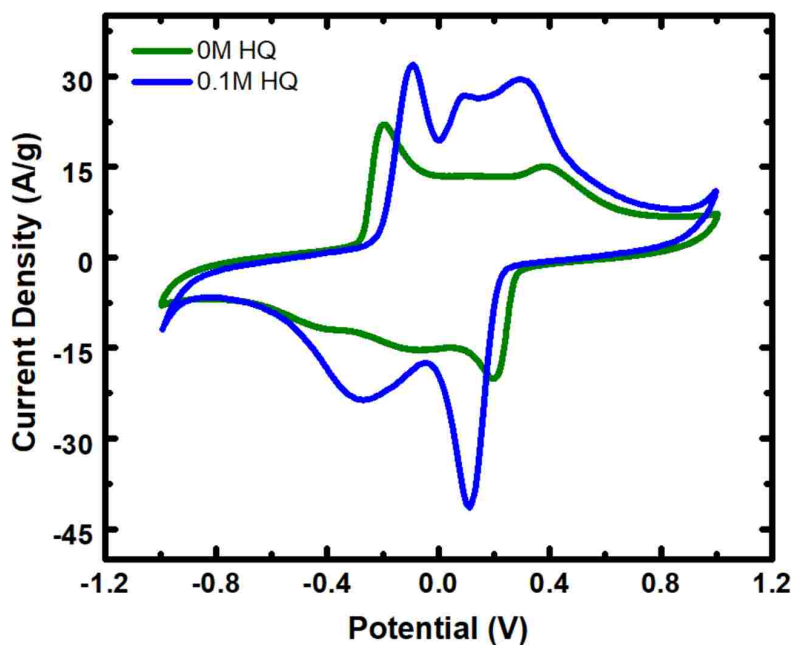
FIG. 25: Cyclic Voltammograms of PANI(1.21V) device at 100 mV/s with and without 0.1M hydroquinone in the liquid electrolyte.

and the electrolyte containing 0.1M hydroquinone to determine how the performance changes in a full-cell build. On average, the performance for the standard electrolyte was about 245 F/g. When the electrolyte with 0.1M hydroquinone was used, the device performance was a little higher with about 368 F/g. A comparison of a device with the standard electrolyte and the hydroquinone electrolyte is shown in Figure 25. It was expected that the current would be higher, even without the redox actions of hydroquinone, since adding hydroquinone to 1M H_2SO_4 increases its conductivity, but the electrochemical activity was greatly enhanced as well. The peaks were all higher and a large peak for hydroquinone appeared. On top of that, the peak separation is reduced when 0.1 HQ is added to the electrolyte. This proves the use of hydroquinone is beneficial for increasing capacitance in a liquid electrolyte full-cell design.

The end goal for this project was to develop a simple manufacturing process to create safe and environmentally friendly supercapacitors. Part of realizing this goal was to implement a solid state electrolyte into the device design even though it may hurt performance. The final iteration was tested with cyclic voltammetry and galvanostatic charge-discharge to fully understand how this device performed when completed.

On average the specific capacitance was about 307 F/g for the fully completed solid state device with hydroquinone. The cyclic voltammogram for an average performing device at 100 mV/s is shown in Figure 26a. The peaks in this sample indicate that the hydroquinone was still able to contribute to energy storage in the PVA electrolyte. Testing the supercapacitor at a lower scan rate of 10 mV/s allows the charge transfer more time to complete, so the peaks do not overlap as they do at 100 mV/s. This is shown in Figure 26b, where the specific capacitance from this scan was 418 F/g. The opposite effect occurs when the scan rate is increased. The peaks overlap and far less energy is able to be stored.
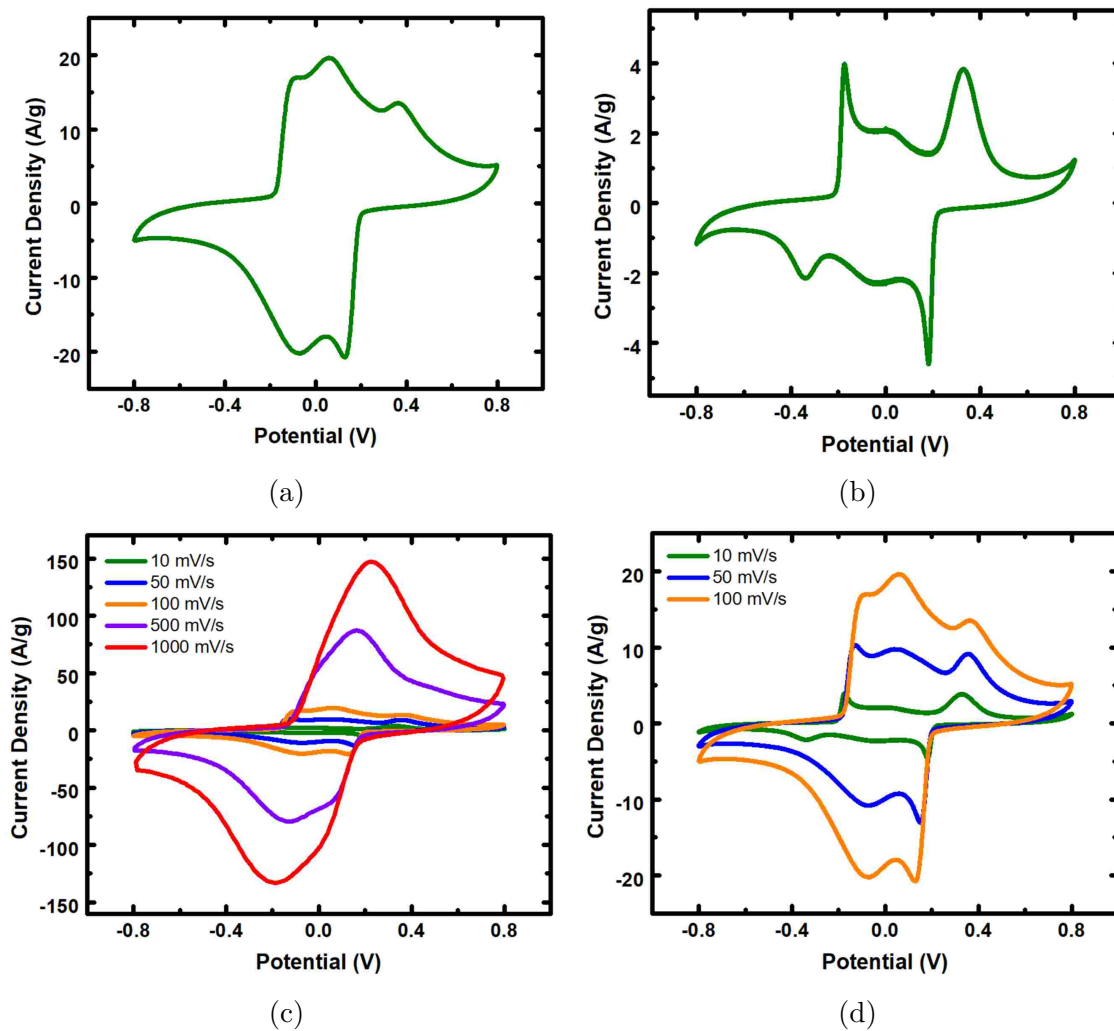
FIG. 26: Cyclic voltammograms of PANI(1.21V) symmetric supercapacitor with solid state PVA electrolate containing 0.1M HQ at scan rates of a) 100 mV/s, b) 10 mV/s, and c) 10, 50, 100, 500, and 1000 mV/s. d) The lower scan rates of 10, 50, and 100 mV/s.
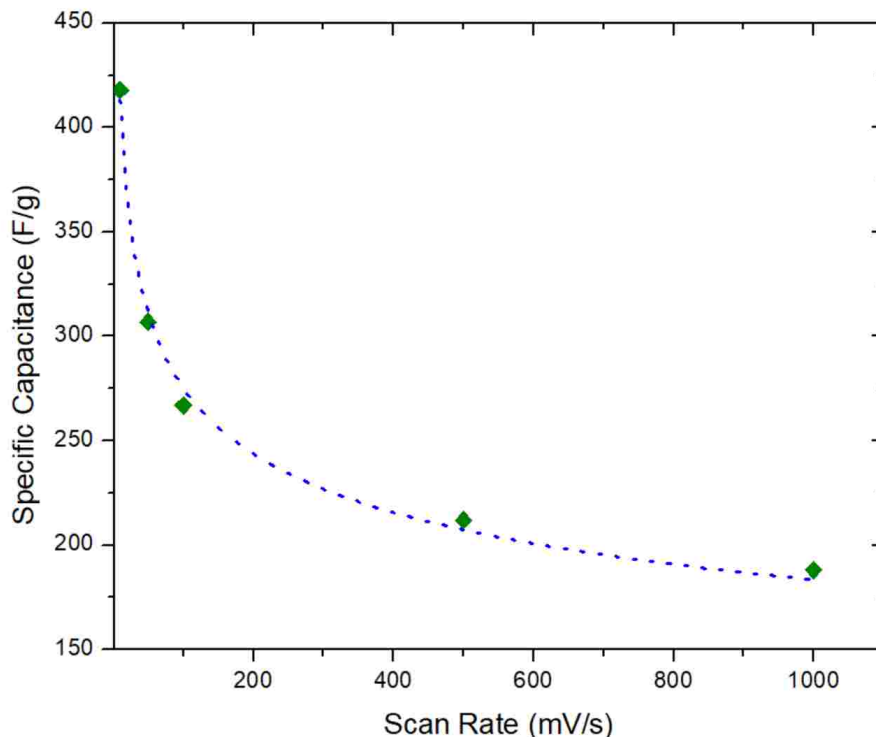
FIG. 27: The specific capacitance of the solid state device as the scan rate is increased.

Other scan rates of 50 mV/s, 500 mV/s, and 1V/s were also tested to understand the dynamic performance. Observe the shape of the response curve as the scan rate is increased to 500 mV/s and 1 V/s as shown in Figure 26c. Eventually the peaks fully overlap into one broad peak, because the redox behavior cannot keep up with the increasing scan rate. At this point the energy stored by hydroquinone is limited by the oxidation of leucoemeraldine to emeraldine. Additionally, Figure 26d is included to show the change in behavior between the three lower scan rates. Using this average device as an example, the estimated performance with a varying scan rate is shown in Figure 27. The performance plummets by over a third as the scan rate is increased from 10 mV/s to 100 mV/s. Increasing the scan rate any higher continues to hurt the specific capacitance, but not nearly as much.

Galvanostatic charge-discharge was also used to test the solid state devices with
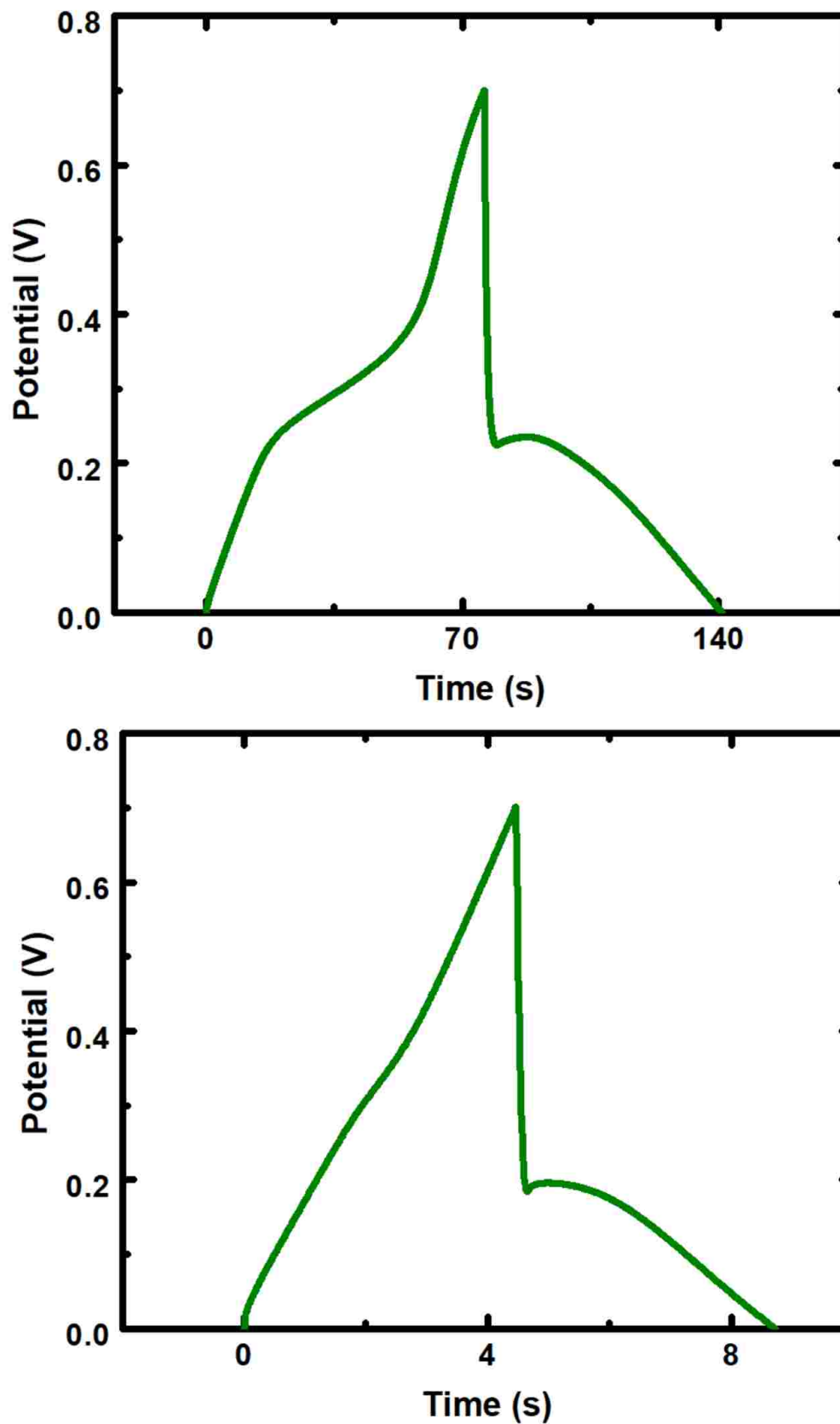
FIG. 28: GCD curves of the symmetric solid state device with PANI(1.21V) and 0.1M HQ in the PVA electrolyte at a) 1 A/g and b) 10 A/g.

hydroquinone in the electrolyte. The average device discussed previously will be used as an example to compare performance between different electrochemical characterization methods. The charge-discharge curve for this device at a current of 1A/g is shown in Figure 28a. The shape is far from the ideal isosceles triangle curve and the charging efficiency was found to be only 85.2% based on the charging and discharging times. The capacitance from this test was found to be 369 F/g at this charging rate. The internal resistance of this supercapacitor is determined to be fairly high at 953 Ω.

This device was found to exhibit 242 F/g at a higher scan rate of 10 A/g. The charge-discharge curve from this test is shown in Figure 28b. The charging behavior is more linear, but the voltage drop upon discharging is even bigger. Interestingly enough, both the resistance and the charging efficiency are better than when tested at 1 A/g. The resistance is only 104 Ω and the efficiency is 95.3%. It is believed that this is due to a high amount of leakage current that causes less self-discharge with a shorter cycle. The cycle for 10 A/g is only about 8.73 seconds, while the cycle is much longer for 1 A/g at 140.83 seconds. A high leakage current can cause the device to lose much more energy in a charging cycle that is nearly 20x as long.

CHAPTER 5

CONCLUSIONS AND FUTURE RESEARCH

5.1 CONCLUSIONS

Polyaniline thin films were fabricated on stainless steel with electropolymerization over a range of voltage to determine the optimal voltage for use as a supercapacitor electrode. It was found that a polyaniline film grown at 1.21V performs the highest under the given conditions. The specific capacitance of electrodes prepared this way exhibited an average of 612 F/g at a scan rate of 100 mV/s. The capacitance was further increased by implementing 0.1M hydroquinone into the electrolyte as a redox mediator. The average specific capacitance attained with this electrolyte was 3,416 F/g in a half-cell. This electrolyte was then tested in a full-cell with a symmetric device structure, and it was found that the performance was 245 F/g on average with 1M H2SO4 electrolyte and 368 F/g when 0.1M hydroquinone was added. The final device iteration involved making a PVA-H2SO4 electrolyte with 0.1M hydroquinone to construct a solid state supercapacitor. The specific capacitance of the final device was about 307 F/g on average.

5.2 FUTURE WORK

This project demonstrated that polyaniline supercapacitors can be fabricated using a two probe electropolymerization process. The overall supercapacitor design and the thin film itself could be further developed in a few ways to improve the design. First, the polyaniline film can be doped with materials other than ions from sulfuric acid to give different effects. Light experimentation was performed to test doping the structure with carbon nanotubes, reduced graphene oxide, graphene oxide,

and cobalt. Perfecting the deposition process with these materials could potentially amplify performance. Another improvement could be with the substrate itself. Conductive carbon nanomaterials could potentially be deposited on the surface of the stainless steel substrate and the polyaniline film can be grown on top to increase the surface area and conductivity. Fabricating this device with a different counter electrode to form an asymmetric supercapacitor could further increase the performance. Additionally the electrolyte could be improved by adding a redox mediator that would work oppositely of hydroquinone. This would allow an asymmetric supercapacitor to experience hydroquinone redox mechanisms on one electrode interface while another redox mediator works on the opposite electrode. The electrode should also be optimized with an organic electrolyte for manufacturing purposes.

Aside from the device structure itself, the fabrication and characterization process could be greatly improved. Properly controlling the environmental constraints and using an electrochemical cell connected to an electrochemical workstation can bring a degree of control that would allow more consistent fabrication. Additionally, this setup could be constructed inside of characterization equipment, such as FTIR, to monitor the growth process in situ. Monitoring the growth process can give a greater understanding of how the film is synthesized. If the growth mechanics are understood well enough, the morphology can be finely tuned by programming a voltage/current curve. The temperature of the precursor solution should also be investigated to understand how the temperature affects the order of film growth.

BIBLIOGRAPHY

[1] G. Yu, X. Xie, L. Pan, Z. Bao, and Y. Cui, "Hybrid nanostructured materials for high-performance electrochemical capacitors," Nano Energy, vol. 2, pp. 213-234, 2013.

[2] G. Z. Chen, "Supercapacitor and supercapattery as emerging electrochemical energy stores," Int. Mater. Rev., vol. 62, no. 4, pp. 173-202, 2017.

[3] B. Conway, Electrochemical Supercapacitors, First. New York: Springer, 1999.

[4] Y. Wang, Y. Song, and Y. Xia, "Electrochemical capacitors: Mechanism, materials, systems, characterization and applications," Chem. Soc. Rev., vol. 45, no. 21, pp. 5925-5950, 2016.

[5] E. Talib and M. A. Azam, An extensive study on carbon nanomaterials electrode from electrophoretic deposition technique for energy storage device, J. Mater. Res., vol. 31, no. 13, pp. 1972-1982, 2016.

[6] C. Zoski, Handbook of Electrochemistry, 1st ed. Amsterdam: Elsevier, 2007.

[7] W. Callister and D. Rethwisch, Materials science and engineering: an introduction, 7th ed., vol. 94. John Wiley & Sons, Inc., 2007.

[8] K. Kiukkola and C. Wagner, "Galvanic Cells for the Determination of the Standard Molar Free Energy of Formation of Metal Halides, Oxides, and Sulfides at Elevated Temperatures," J. Electrochem. Soc., vol. 104, no. 5, p. 308, 1957.

[9] M. Faraday, "Experimental Researches in Electricity," Philos. Trans., vol. 96, no. 124, pp. 77-122, 1834.

[10] F. C. Walsh, "Overall rates of electrode reactions. Faradays Laws of Electrolysis," Trans. Inst. Met. Finish., vol. 69, no. pt 4, pp. 155-157, 1991.

[11] S. Zhang and N. Pan, "Supercapacitors performance evaluation," Adv. Energy Mater., vol. 5, no. 6, pp. 1-19, 2015.

[12] H. Li, J. Wang, Q. Chu, Z. Wang, F. Zhang, and S. Wang, "Theoretical and experimental specific capacitance of polyaniline in sulfuric acid," J. Power Sources, vol. 190, no. 2, pp. 578-586, 2009.

[13] L. L. Zhang and X. S. Zhao, "Carbon-based materials as supercapacitor electrodes," Chem. Soc. Rev., vol. 38, no. 9, pp. 2520-2531, 2009.

[14] R. Chen, L. Liu, J. Zhou, L. Hou, and F. Gao, "High-performance nickel-cobalt-boron material for an asymmetric supercapacitor with an ultrahigh energy density," J. Power Sources, vol. 341, pp. 7582, 2017.

[15] Z. Liu, H. Zhang, Q. Yang, and Y. Chen, "Graphene / V2O5hybrid electrode for an asymmetric supercapacitor with high energy density in an organic electrolyte," Electrochim. Acta, pp. 210, 2018.

[16] S. S. Zhang, "Eliminating pre-lithiation step for making high energy density hybrid Li-ion capacitor," J. Power Sources, vol. 343, pp. 322-328, 2017.

[17] P. Kurzweil, Post–lithium–ion battery chemistries for hybrid electric vehicles and battery electric vehicles. 2015.

[18] W. Wang et al., "Hydrous ruthenium oxide nanoparticles anchored to graphene and carbon nanotube hybrid foam for supercapacitors," Sci. Rep., vol. 4, no. ii, pp. 9-14, 2014.

[19] A. Ghosh, V. T. Le, J. J. Bae, and Y. H. Lee, "TLM–PSD model for optimization of energy and power density of vertically aligned carbon nanotube supercapacitor," Sci. Rep., vol. 3, pp. 1-10, 2013.

[20] S. Haber, "Deep electrophoretic penetration and deposition of ceramic particles inside impermeable porous substrates," J. Colloid Interface Sci., vol. 179, no. 2, pp. 380-390, 1996.

[21] P. Guillemet, T. Brousse, O. Crosnier, Y. Dandeville, L. Athouel, and Y. Scudeller, "Modeling pseudo capacitance of manganese dioxide," Electrochim. Acta, vol. 67, pp. 41-49, 2012.

[22] A. B. Rohom, P. U. Londhe, S. K. Mahapatra, S. K. Kulkarni, and N. B. Chaure, "Electropolymerization of polyaniline thin films," High Perform. Polym., vol. 26, no. 6, pp. 641646, 2014.

[23] A. Eftekhari, L. Li, and Y. Yang, "Polyaniline supercapacitors," J. Power Sources, vol. 347, pp. 86-107, 2017.

[24] S. Abdulla, T. L. Mathew, and B. Pullithadathil, "Highly sensitive, room temperature gas sensor based on polyaniline-multiwalled carbon nanotubes (PANI/MWCNTs) nanocomposite for trace-level ammonia detection," Sensors Actuators, B Chem., vol. 221, pp. 1523-1534, 2015.

[25] Q. Liu et al., "Preparation of PAA-g-PEG/PANI Polymer Gel Electrolyte and Its Application in Quasi Solid State Dye–Sensitized Solar Cells," Polym. Eng. Sci., vol. 55, pp. 322-326, 2014.

[26] M. F. Zainal, Y. Mohd, and R. Ibrahim, "Preparation and Characterization of Electrochromic Polyaniline (PANi) Thin Films," IEEE Bus. Eng. Ind. Appl. Colloq., no. 13672771, pp. 64-68, 2013.

[27] A. G. MacDiarmid and A. J. Epstein, "Polyaniline: A Novel Class of Conducting Polymers," Faraday Disc., vol. 88, pp. 317-331, 1989.

[28] A. G. Macdiarmid and J. Chiang, "Polyaniline: Protonic Acid Doping of the Emeraldine Form to the Metallic Regime," Synth. Met., vol. 13, pp. 193-205, 1986.

[29] M. Magnuson et al., "The electronic structure of polyaniline and doped phases studied by soft x-ray absorption and emission spectroscopies," J. Chem. Phys., vol. 111, no. 10, pp. 4756-4761, 1999.

[30] L. W. Shacklette, "Dipole and hydrogen-bonding interactions in polyaniline: mechanism for conductivity enhancement," Synth. Met., vol. 65, pp. 123-130, 1994.

[31] M. M. Ostwal, J. Pellegrino, I. Norris, T. T. Tsotsis, M. Sahimi, and B. R. Mattes, "Water Sorption of Acid-Doped Polyaniline Solid Fibers: Equilibrium and Kinetic Response," Ind. Eng. Chem. Res., vol. 44, pp. 7860-7867, 2005.

[32] E. Song and J.-W. Choi, "Conducting Polyaniline Nanowire and Its Applications in Chemiresistive Sensing," Nanomaterials, vol. 3, no. 3, pp. 498-523, 2013.

[33] Y. Cao, "Spectroscopic studies of acceptor and donor doping of polyaniline in the emeraldine base and pernigraniline forms," Synth. Met., vol. 35, no. 3, pp. 319-332, 1990.

[34] A. G. Macdiarmid et al., "Polyaniline: Interconversion of Metallic and Insulating Forms," Mol. Cryst. Liq. Cryst., vol. 121, pp. 173-180, 1985.

[35] W. R. Salaneck, I. Lundstrom, W. Huang, and A. G. Macdiarmid, "A two-dimensional-surface state diagram for polyaniline," Synth. Met., vol. 13, pp. 291297, 1986.

[36] H. Xu, J. Tang, Y. Chen, J. Liu, J. Pu, and Q. Li, "Zn2+-Doped Polyaniline/Graphene Oxide as Electrode Material for Electrochemical Supercapacitors," J. Electron. Mater., vol. 46, no. 10, pp. 61506157, 2017.

[37] T. Wu and Y. Lin, "Doped polyaniline/multi-walled carbon nanotube composites: Preparation, characterization and properties," Polymer, vol. 47, pp. 35763582, 2006.

[38] A. Macdiarmid, S. Manohar, J. Masters, Y. Sun, H. Weiss, and A. Epsten, "Polyaniline: synthesis and properties of pernigraniline base," Synth. Met., vol. 41, pp. 621626, 1991.

[39] N. M. Rowley and R. J. Mortimer, "New electrochromic materials.," Sci. Prog., vol. 85, no. Pt 3, pp. 243262, 2002.

[40] C. M. S. Izumi, V. R. L. Constantino, A. M. C. Ferreira, and M. L. A. Temperini, "Spectroscopic characterization of polyaniline doped with transition metal salts," Synth. Met., vol. 156, pp. 654663, 2006.

[41] K. Bienkowski, "Polyaniline and its derivatives doped with Lewis acids- synthesis and spectroscopic properites," Warsaw University of Technology, 2006.

[42] J. Stejskal, P. Kratochvil, and A. D. Jenkins, "The formation of polyaniline and the nature of its structures," Polymer, vol. 37, no. 2, pp. 367-369, 1996.

[43] L. Pan, L. Pu, Y. Shi, T. Sun, R. Zhang, and Y. Zheng, "Hydrothermal synthesis of polyaniline mesostructures," Adv. Funct. Mater., vol. 16, no. 10, pp. 1279-1288, 2006.

[44] Y. Cao, A. Andreatta, A. J. Heeger, and P. Smith, "Influence of chemical polymerization conditions on the properties of polyaniline," Polymer, vol. 30, no. 12, pp. 23052311, 1989.

[45] S. Bhadra, D. Khastgir, N. K. Singha, and J. Hee, "Progress in preparation, processing and applications of polyaniline," Prog. Polym. Sci., vol. 34, pp. 783-810, 2009.

[46] G. Wallace, G. Spinks, L. Kane-Maguire, and P. Teasdale, Conductive Electroactive Polymers: Intelligent Polymer Systems, Third. Boca Raton: CRC Press, 2009.

[47] R. Waltman and J. Bargon, "Electrically conducting polymers: a review of the electropolymerization reaction, of the effects of chemical structure on polymer film properties, and of applications towards technology," Can. J. Chem., vol. 64, pp. 76-95, 1986.

[48] E. Genies, A. Syed, and C. Tsintavis, "Electrochemical Study Of Polyaniline In Aqueous And Organic Medium. Redox And Kinetic Properties.," Mol. Cryst. Liq. Cryst., vol. 121, pp. 181186, 1985.

[49] N. Yi and M. R. Abidian, Conducting polymers and their biomedical applications. 2015.

[50] D. E. Stilwell and S. Park, "Electrochemistry of Conductive Polymers: II. Electrochemical Studies on Growth Properties of Polyaniline," J. Electrochem. Soc., vol. 135, no. 9, pp. 2254-2262, 1988.

[51] M. Leclerc, J. Guay, and L. Dao, "Synthesis and Characterization of Poly(alkylanilines)," Macromolecules, vol. 22, pp. 649-653, 1989.

[52] Y. Wu, J. Wang, B. Ou, S. Zhao, Z. Wang, and S. Wang, "Electrochemical Preparation of Polyaniline Nanowires with the Used Electrolyte Solution Treated with the Extraction Process and Their Electrochemical Performance," Nanomaterials, vol. 8, p. 103, 2018.

[53] H. H. Tan, K. G. Neoh, F. T. Liu, N. Kocherginsky, and E. T. Kang, "Crosslinking and Its Effects on Polyaniline Films," J. Appl. Polym. Sci., vol. 80, pp. 1-9, 2001.

[54] J. C. Cooper and E. A. H. Hall, "Catalytic reduction of benzoquinone at polyaniline and polyaniline/enzyme films," Electroanalysis, vol. 5, no. 56, pp. 385397, 1993.

[55] S. Roldn, M. Granda, R. Menndez, R. Santamara, and C. Blanco, "Mechanisms of energy storage in carbon-based supercapacitors modified with a quinoid redox-active electrolyte," J. Phys. Chem. C, vol. 115, no. 35, pp. 1760617611, 2011.

[56] S. Senthilkumar, R. Selvan, and J. Melo, "Redox additive/active electrolytes: a novel approach to enhance the performance of supercapacitors," J. Mater. Chem. A, vol. 1, no. 40, pp. 1238612394, 2013.

[57] Q. Li, K. Li, C. Sun, and Y. Li, "An investigation of $Cu2+$ and $Fe2+$ ions as active materials for electrochemical redox supercapacitors," J. Electroanal. Chem., vol. 611, pp. 4350, 2007.

[58] L. Duic and S. Grigic, "The effect of polyaniline morphology on hydroquinone/quinone redox reaction," Electrochim. Acta, vol. 46, no. 18, pp. 27952803, 2001.

[59] E. S. Matveeva, I. Hernndez-Fuentes, V. Parkhutik, and R. Daz-Calleja, "Direct involvement of acid centers of polyaniline in charge transfer on organic acceptor," Synth. Met., vol. 83, no. 3, pp. 181184, 1996.

[60] E. S. Matveeva, "Could the acid doping of polyaniline represent the charge transfer interaction?," Synth. Met., vol. 83, no. 2, pp. 8996, 1996.

[61] V. V. N. Obreja, A. Dinescu, and A. C. Obreja, "Activated carbon based electrodes in commercial supercapacitors and their performance," Int. Rev. Electr. Eng., vol. 5, pp. 272282, 2010.

[62] C. Zhong, Y. Deng, W. Hu, J. Qiao, L. Zhang, and J. Zhang, "A review of electrolyte materials and compositions for electrochemical supercapacitors," Chem. Soc. Rev., vol. 44, no. 21, pp. 74847539, 2015.

[63] G. Wang, L. Zhang, and J. Zhang, "A review of electrode materials for electrochemical supercapacitors," Chem. Soc. Rev., vol. 41, pp. 797828, 2012.

[64] N. H. Khdary, M. E. Abdesalam, and G. EL Enany, "Mesoporous Polyaniline Films for High Performance Supercapacitors," J. Electrochem. Soc., vol. 161, no. 9, pp. G63G68, 2014.

[65] D. S. Dhawale, A. Vinu, and C. D. Lokhande, "Stable nanostructured polyaniline electrode for supercapacitor application," Electrochim. Acta, vol. 56, no. 25, pp. 94829487, 2011.

[66] P. Sivaraman et al., "All solid supercapacitor based on polyaniline and crosslinked sulfonated poly[ether ether ketone]," Electrochim. Acta, vol. 55, no. 7, pp. 24512456, 2010.

[67] A. Samantara and S. Ratha, Materials Development for Active/Passive Components of a Supercapacitor. Springer, 2018.

[68] M. Kaempgen, C. K. Chan, J. Ma, Y. Cui, and G. Gruner, "Printable Thin Film Supercapacitors Using Single-Walled Carbon Nanotubes," Nano Lett., vol. 9, pp. 18721876, 2009.

[69] J. M. D. Rodrguez, J. Alberto, H. Melin, and J. P. Pea, "Determination of the Real Surface Area of Pt Electrodes by Hydrogen Adsorption Using Cyclic Voltammetry," J. Chem. Educ., vol. 77, no. 9, pp. 11951197, 2000.

[70] S. N. Inamdar, P. P. Ingole, and S. K. Haram, "Determination of Band Structure Parameters and the Quasi-Particle Gap of CdSe Quantum Dots by Cyclic Voltammetry," ChemPhysChem, vol. 9, pp. 25742579, 2008.

[71] G. A. Mabbott, "An Introduction to Cyclic Voltammetry," J. Chem. Educ., vol. 60, no. 9, pp. 697702, 1983.

[72] G. Zhang, W. Li, K. Xie, F. Yu, and H. Huang, "A One-Step and Binder-Free Method to Fabricate Hierarchical Nickel-Based Supercapacitor Electrodes with Excellent Performance," Adv. Funct. Mater., vol. 23, pp. 36753681, 2013.

[73] R. Zhang, D. Harrison, J. Fyson, F. Qiu, and D. Southee, "Flexible Strip Supercapacitors for Future Energy Storage," Int. J. Autom. Comput., vol. 12, pp. 4349, 2015.

[74] M. Arulepp et al., "Influence of the solvent properties on the characteristics of a double layer capacitor," J. Power Sources, vol. 133, pp. 320328, 2004.

[75] Z. J. Zhang, C. Dong, X. Y. Ding, and Y. K. Xia, "A generalized ZnCl2 activation method to produce nitrogen-containing nanoporous carbon materials for supercapacitor applications," J. Alloys Compd., vol. 636, pp. 275281, 2015.

[76] A. Laher, P. Przygocki, Q. Abbas, and F. Bguin, "Appropriate methods for evaluating the efficiency and capacitive behavior of different types of supercapacitors," Electrochem. commun., vol. 60, pp. 2125, 2015.

[77] M. D. Stoller and R. S. Ruoff, "Best practice methods for determining an electrode materials performance for ultracapacitors," Energy Environ. Sci., vol. 3, no. 9, pp. 12941301, 2010.

[78] V. Augustyn, B. Dunn, and P. Simon, "Pseudocapacitive oxide materials for high-rate electrochemical energy storage," Energy Environ. Sci., vol. 7, pp. 15971614, 2014.

[79] A. S. Adekunle, K. I. Ozoemena, B. B. Mamba, B. O. Agboola, and O. Oluwatobi, "Supercapacitive Properties of Symmetry and the Asymmetry Two Electrode Coin Type Supercapacitor Cells Made from MWCNTS/Nickel Oxide Nanocomposite," Int. J. Electrochem. Sci., vol. 6, pp. 47604774, 2011.

[80] A. Ramadoss and S. Kim, "Vertically aligned TiO2 nanorod arrays for electrochemical supercapacitor," J. Alloys Compd., vol. 561, pp. 262267, 2013.

[81] B. K. Kim, S. Sy, A. Yu, and J. Zhang, "Electrochemical Supercapacitors for Energy Storage and Conversion," Handbook of Clean Energy Systems, 2015.

[82] S. Ban, J. Zhang, L. Zhang, K. Tsay, D. Song, and X. Zou, "Charging and discharging electrochemical supercapacitors in the presence of both parallel leakage process and electrochemical decomposition of solvent," Electrochim. Acta, vol. 90, pp. 542549, 2013.

[83] T. Shinomiya, V. Gupta, and N. Miura, "Effects of electrochemical-deposition method and microstructure on the capacitive characteristics of nano-sized manganese oxide," Electrochim. Acta, vol. 51, no. 21, pp. 44124419, 2006.

[84] Y. Z. Zhang, Y. Wang, T. Cheng, W. Y. Lai, H. Pang, and W. Huang, "Flexible supercapacitors based on paper substrates: a new paradigm for low-cost energy storage," Chem. Soc. Rev., vol. 44, no. 15, pp. 51815199, 2015.

[85] C. P. Fonseca, J. E. Benedetti, and S. Neves, "Poly(3-methyl thiophene)/PVDF composite as an electrode for supercapacitors," J. Power Sources, vol. 158, no. 1, pp. 789794, 2006.

[86] X. Yang, L. Zhang, F. Zhang, T. Zhang, Y. Huang, and Y. Chen, "A high-performance all-solid-state supercapacitor with graphene-doped carbon material electrodes and a graphene oxide-doped ion gel electrolyte," Carbon N. Y., vol. 72, pp. 381386, 2014.

[87] K. Subramani, N. Sudhan, R. Divya, and M. Sathish, "All-solid-state asymmetric supercapacitors based on cobalt hexacyanoferrate-derived CoS and activated carbon," RSC Adv., vol. 7, no. 11, pp. 66486659, 2017.

[88] N. B. Colthup, L. H. Daly, and S. E. Wiberley, Introduction to Infrared and Raman Spectroscopy, Third. San Diego: Academic Press inc., 1990.

[89] P. Griffiths and J. Haseth, Fourier Transform Infrared Spectrometry, Second. Hoboken: John Wiley & Sons, Inc., 2007.

[90] J. I. Goldstein, D. E. Newbury, J. R. Michael, N. W. M. Ritchie, J. H. J. Scott, and D. C. Joy, Scanning Electron Microscopy and X-Ray Microanalysis, 4th ed. 2018.

[91] D. K. Schroder, Semiconductor Material and Device Characterization. 2006.

[92] M. Kaya, I. Sargin, I. Al-jaf, S. Erdogan, and G. Arslan, "Characteristics of corneal lens chitin in dragonfly compound eyes," Int. J. Biol. Macromol., vol. 89, pp. 5461, 2016.

[93] M. Gao, G. Zhang, G. Zhang, X. Wang, S. Wang, and Y. Yang, "The resistance to over-oxidation for polyaniline initiated by the resulting quinone-like molecules," Polym. Degrad. Stab., vol. 96, no. 10, pp. 17991804, 2011.

[94] G. Sand and P. Vansek, "Impedance and voltammetric studies of electrogenerated polyaniline conducting films," Synth. Met., vol. 64, no. 1, pp. 18, 1994.

[95] A. Baba et al., "Electropolymerization and doping/dedoping properties of polyaniline thin films as studied by electrochemical-surface plasmon spectroscopy and by the quartz crystal microbalance," J. Electroanal. Chem., vol. 562, no. 1, pp. 95103, 2004.

[96] Z. Morvkov and E. Dmitrieva, "Structural changes in polyaniline near the middle oxidation peak studied by in situ Raman spectroelectrochemistry," J. Raman Spectrosc., vol. 48, no. 9, pp. 12291234, 2017.

[97] E. Dmitrieva, Y. Harima, and L. Dunsch, "Influence of phenazine structure on polaron formation in polyaniline: in situ electron spin resonance-Ultraviolet/visible-Near-Infrared spectroelectrochemical study," J. Phys. Chem. B, vol. 113, no. 50, pp. 1613116141, 2009.

[98] C. H. Choi and M. Kertesz, "Conformational studies of vibrational properties and electronic states of leucoemeraldine base and its oligomers," Macromolecules, vol. 30, no. 3, pp. 620630, 1997.

[99] S. Gul, A. U. H. A. Shah, and S. Bilal, "Synthesis and characterization of processable polyaniline salts," J. Phys. Conf. Ser., vol. 439, no. 1, 2013.

[100] Y. Xia, J. M. Wiesinger, A. G. MacDiarmid, and A. J. Epstein, "Camphorsulfonic Acid Fully Doped Polyaniline Emeraldine Salt: Conformations in Different Solvents Studied by an Ultraviolet/Visible/ Near-Infrared Spectroscopic Method," Chem. Mater., vol. 7, no. 3, pp. 443445, 1995.

[101] A. G. M. and A. J. Epstein, Polyaniline: Synthesis, chemistry, and processing, pp. 112, 1992.

[102] Z. Moravkova, J. Stejskal, M. Trchova, and I. Sedenkova, "Spectroscopy of thin film polyaniline films deposited during chemical oxidation of aniline," Chem. Pap. Slovac Acad. Sci., vol. 66, pp. 415445, 2012.

[103] X. Wei, Y. Z. Wang, S. M. Long, C. Bobeczko, and A. J. Epstein, "Synthesis and Physical Properties of Highly Sulfonated Polyaniline," J. Am. Ceram. Soc., vol. 118, pp. 25452555, 1996.

[104] E. M. Elnaggar, H. S. Elsherif, and M. A. Migahed, "Nano Reactive Polymer as Asphalt Modifier for Anticorrosion Application," J. Nanosci. Nanoeng., vol. 1, pp. 917, 2015.

[105] M. G. Han, S. K. Cho, S. G. Oh, and S. S. Im, "Preparation and characterization of polyaniline nanoparticles synthesized from DBSA micellar solution," Synth. Met., vol. 126, pp. 5360, 2002.

[106] M. D. Bedre, R. Deshpande, B. Salimath, and V. Abbaraju, "Preparation and Characterization of Polyaniline-Co3O4 Nanocomposites via Interfacial Polymerization," Am. J. Mater. Sci., vol. 2, no. 3, pp. 3943, 2012.

[107] B. C. Kim, H. T. Jeong, C. J. Raj, Y. R. Kim, B. B. Cho, and K. H. Yu, "Electrochemical performance of flexible poly(ethylene terephthalate) (PET) supercapacitor based on reduced graphene oxide (rGO)/single-wall carbon nanotubes (SWNTs)," Synth. Met., vol. 207, pp. 116121, 2015.

[108] G. Wang, R. Liang, L. Liu, and B. Zhong, "Improving the specific capacitance of carbon nanotubes-based supercapacitors by combining introducing functional groups on carbon nanotubes with using redox-active electrolyte," Electrochim. Acta, vol. 115, pp. 183188, 2014.

APPENDIX A

PERMISSIONS

The following copyright permissions were obtained for legal reproduction or adaptation of previously published figures for use in this work:

The graphic used for Figure 7 comes from a publication by Hall and Cooper [205].

The graphics used for Figure 9 comes from a publication by Ban, et al. [144].

The graphic used for Figure 10 comes from a publication by Kaya, et al. [124].

The permission receipts are included on the following pages.

This Agreement between Jonathan R Blincoe ("You") and John Wiley and Sons ("John Wiley and Sons") consists of your license details and the terms and conditions provided by John Wiley and Sons and Copyright Clearance Center.

License Number	4465080720882
License date	Nov 09, 2018
Licensed Content Publisher	John Wiley and Sons
Licensed Content Publication	Electroanalysis
Licensed Content Title	Catalytic reduction of benzoquinone at polyaniline and polyaniline/enzyme films
Licensed Content Author	Elizabeth A. H. Hall, Julia C. Cooper
Licensed Content Date	Apr 9, 2005
Licensed Content Volume	5
Licensed Content Issue	5-6
Licensed Content Pages	13
Type of use	Dissertation/Thesis
Requestor type	University/Academic
Format	Print and electronic
Portion	Figure/table
Number of figures/tables	2
Original Wiley figure/table number(s)	Scheme 1, Scheme 4
Will you be translating?	No
Title of your thesis / dissertation	SOLID STATE POLYANILINE SUPERCAPACITORS BASED ON ELECTRODES FABRICATED WITH ELECTROPOLYMERIZATION
Expected completion date	Dec 2018
Expected size (number of pages)	100
Requestor Location	Jonathan R Blincoe 5200 Foxboro Landing
	Virginia Beach, VA 23464 United States Attn:
Publisher Tax ID	EU826007151
Total	0.00 USD
Terms and Conditions	

ELSEVIER LICENSE
TERMS AND CONDITIONS

Nov 09, 2018

This Agreement between Jonathan R Blincoe ("You") and Elsevier ("Elsevier") consists of your license details and the terms and conditions provided by Elsevier and Copyright Clearance Center.

License Number	4465071407775
License date	Nov 09, 2018
Licensed Content Publisher	Elsevier
Licensed Content Publication	Electrochimica Acta
Licensed Content Title	Charging and discharging electrochemical supercapacitors in the presence of both parallel leakage process and electrochemical decomposition of solvent
Licensed Content Author	Shuai Ban,Jiujun Zhang,Lei Zhang,Ken Tsay,Datong Song,Xinfu Zou
Licensed Content Date	Feb 15, 2013
Licensed Content Volume	90
Licensed Content Issue	n/a
Licensed Content Pages	8
Start Page	542
End Page	549
Type of Use	reuse in a thesis/dissertation
Portion	figures/tables/illustrations
Number of figures/tables /illustrations	2
Format	both print and electronic
Are you the author of this Elsevier article?	No
Will you be translating?	No
Original figure numbers	Figure 2, Figure 4
Title of your thesis/dissertation	SOLID STATE POLYANILINE SUPERCAPACITORS BASED ON ELECTRODES FABRICATED WITH ELECTROPOLYMERIZATION
Expected completion date	Dec 2018
Estimated size (number of pages)	100
Requestor Location	Jonathan R Blincoe 5200 Foxboro Landing Virginia Beach, VA 23464 United States Attn:
Publisher Tax ID	98-0397604
Total	0.00 USD
Terms and Conditions	

ELSEVIER LICENSE
TERMS AND CONDITIONS

Nov 09, 2018

This Agreement between Jonathan R Blincoe ("You") and Elsevier ("Elsevier") consists of your license details and the terms and conditions provided by Elsevier and Copyright Clearance Center.

License Number	4465070863391
License date	Nov 09, 2018
Licensed Content Publisher	Elsevier
Licensed Content Publication	International Journal of Biological Macromolecules
Licensed Content Title	Characteristics of corneal lens chitin in dragonfly compound eyes
Licensed Content Author	Murat Kaya,Idris Sargin,Ivan Al-jaf,Sevil Erdogan,Gulsin Arslan
Licensed Content Date	Aug 1, 2016
Licensed Content Volume	89
Licensed Content Issue	n/a
Licensed Content Pages	8
Start Page	54
End Page	61
Type of Use	reuse in a thesis/dissertation
Intended publisher of new work	other
Portion	figures/tables/illustrations
Number of figures/tables /illustrations	1
Format	both print and electronic
Are you the author of this Elsevier article?	No
Will you be translating?	No
Original figure numbers	Figure 2.b
Title of your thesis/dissertation	SOLID STATE POLYANILINE SUPERCAPACITORS BASED ON ELECTRODES FABRICATED WITH ELECTROPOLYMERIZATION
Expected completion date	Dec 2018
Estimated size (number of pages)	100
Requestor Location	Jonathan R Blincoe 5200 Foxboro Landing Virginia Beach, VA 23464 United States Attn:
Publisher Tax ID	98-0397604
Total	0.00 USD
Terms and Conditions	

VITA

Jonathan R. Blincoe

Department of Electrical and Computer Engineering

Old Dominion University

Norfolk, VA 23529

EDUCATION:

Bachelor of Science- Electrical Engineering and Computer Engineering

Old Dominion University- Fall 2016

Norfolk, VA

BACKGROUND OF STUDY:

My undergraduate studies were focused on building a complete understanding of electronics and computers through a double major in computer engineering and electrical engineering with a minor in computer science. During this time I also worked as the IT Manager in a healthcare facility, which helped me gain hands on experience and develop real skills for system/resource management and administrative duties. I completed my Bachelor of Science in May 2016. After a semester-long break, I returned to Old Dominion University to attain a Master of Science focused on Electrical Engineering. I learned to fabricate perovskite solar cells and supercapacitors before then delving into publications to learn about nanomaterials used for energy generation and storage. I studied fabrication methods to make useful nanomaterials and the how the properties are affected by changes in the fabrication method. Supercapacitors were then constructed using various nanomaterials including carbon nanotubes, graphene oxide, reduced graphene oxide, carbon nanofoam, activated carbon, manganese oxide, and polyaniline.

Typeset using LaTeX.